UNIVERSIDADE D
COIMBRA

Pedro Rafael Lopes Castelhanito

LICK & RUN:

IDENTIFYING BEHAVIORAL MODULATION IN CEREBELLAR PURKINJE CELLS

Dissertação no âmbito do Mestrado em Biologia Celular e Molecular – Especialização em Neurobiologia orientada pela Doutora Megan R. Carey, com orientação interna do Professor Doutor João Peça e apresentada ao Departamento de Ciências da Vida da Faculdade de Ciências e Tecnologia da Universidade de Coimbra

Novembro de 2021

Abstract

The cerebellum is a key brain structure to execute smooth, coordinated movements. Although a lot is known about the anatomical organization of the cerebellar cortex, we still don't have a clear view of how different information converges and is represented within this circuit to allow for whole-body coordination. In this project, we performed cell-attached recordings of Purkinje cells in mice during head-fixed locomotion and licking, to identify and quantify the different representations of behavior in single cells. For this dissertation we only focused on the analyses conducted to identify and quantify licking-related modulations. In accordance with previous studies, our time alignment analysis demonstrated two types of licking-related cell responses: single lick and lick bout modulation. However, we identified a correlation between lick bout onsets and locomotion speed variation in our dataset which could not be disentangled with the previous method. To minimize this confounding correlation, we quantified the contributions of speed, single licks and lick bouts to the firing rate of the cell, through Generalized Additive Models. We found that most cells were speed modulated and that, simultaneously, single lick and lick bout modulation were equally present in our population, sometimes exhibiting the three types of modulation at the same time. We also performed preliminary analysis that suggest a weak relationship between the cell anatomical locations and their modulations. Altogether, these results demonstrate that single Purkinje cells encode combined behavioral representations of at least two different behaviors: licking and locomotion, which might be related to their position within the cerebellum.

keywords: *Cerebellum, Purkinje cells, licking behavior, modulation quantification*

Resumo

O cerebelo é uma área chave do nosso cérebro na execução de movimentos coordenados. Ainda que o conhecimento sobre a organização anatómica do cortex cerebelar seja extenso, pouco se sabe sobre como informaçoes diferentes convergem e são representadas neste circuito, possibilitando a coordenação de todo o corpo. Neste projeto, realizámos gravações eletrofisiológicas de células Purkinje em murganhos durante locomoção e consumo de água com cabeça imobilizada, para identificar e quantificar diferentes representações de comportamento em células individuais. Esta dissertação foca-se apenas na análise realizada para identificar e quantificar modulações associadas ao consumo de água. Assim como na literatura, identificámos dois tipos de resposta por parte das células: uma associada a movimentos de língua individuais e outra associada ao consumo de água no geral. Contudo, identificámos nos nossos dados uma correlação entre o início de consumo de água e variações de velocidade de locomoção, em que o método anterior não é capaz de destrinçar. Para minimizar o efeito desta correlação, quantificámos as contribuições individuais da velocidade, movimentos individuais da língua e consumo de água na atividade da célula, através de Modelos Aditivos Generalizados. Identificámos que a maioria das células são moduladas pela velocidade de locomoção e que, simultaneamente, os dois tipos de modulações associadas ao consumo de água estão igualmente representadas na nossa população, por vezes havendo células que possuem os três tipos de modulação ao mesmo tempo. Também realizámos uma análise preliminária que sugere uma relação fraca entre a localização anatómica das células e as suas modulações. Resumindo, estes resultados demonstram que células Purkinje individuais codificam combinações de representações de pelo menos dois comportamentos: locomoção e consumo de água, e que estas podem estar relacionadas com a sua posição no cerebelo.

Palavras chave: *Cerebelo, células Purkinje, consumo de água, quantificação de modulação*

Acknowledgements

First of all, I would like to thank Dr. Megan Carey for providing me one of the best experiences I've ever had, for all the feedback, for the support, and for really caring about her team. Then, I would like to specially thank Dr. Hugo Marques and Dr. Jorge Ramirez for all their incredible work mentoring me. Thank you for all the answered questions, for all the discussions, for all your help, and for all the moments we worked together, it did not go unnoticed. I really hope I can one day be to someone who you were to me.

To all the lab, thank you for all the amazing moments we shared. Thank you for all the beers and caipirinhas, for all the bad next mornings, for all the advices and specially for having to listen to me sing in the open lab. You made this experience be incredible, I owe that to you. I would like to mention and thank Jovin for all the afternoons lost in just a "quick snack", afternoons that felt like the predicted 15 minutes but that I will keep forever.

Gostaria também de deixar um agradecimento especial à minha família por me ter acompanhado durante todo este tempo. Obrigado por possibilitarem tudo, e mais, que o necessário para poder estar aqui e ser quem sou. Nada seria possível sem vocês.

Index

List of Figures

List of abbreviations

AP, Anterior-Posterior

BM, Bout Modulated

CS, Complex Spikes

CF, Climbing fiber

DCN, Deep Cerebellar Nuclei

DLC, DeepLabCut

DV, Dorso-Ventral

ED, Experimental distance

GAM, Generalized Additive Model

GMI, GAM Modulation Index

HD, Histology distance

ISI, Inter-spike interval

LM, Lick Modulated

MI, Modulation Index

ML, Medio-Lateral

NM, Non-Modulated

PC, Purkinje cell

PD, Partial dependency

PF, Parallel fiber

SS, Simple Spikes

SM, Speed Modulated

1. Introduction

The cerebellum is crucial for the execution and control of motor outputs. Its characteristically regular and stereotypic circuitry provides the substrate to infer that the cerebellum functions in a uniform computational framework (Apps, Hawkes, 2009). Despite its highly modular architecture, one of the long-standing challenges has been to understand the computational rules that govern the activity of this structure. For this, we first need to understand how information is encoded and processed during behavior in the cerebellar circuitry.

1.1 Anatomy & structure of the cerebellar cortex

The cerebellum can be divided into 2 main regions: the cerebellar cortex and the deep cerebellar nuclei (DCN). The first is thought to be responsible for information processing, while the latter serves as the cerebellar output pathway, conveying the readout to many cortical and peripheral targets (Purves et al., 2017).

The cerebellar cortex is the largest receptacle of inputs to the cerebellum. It is thought that this information is topographically represented throughout the cerebellar structure, organizing somatomotor information according to its source of input (Snider, Stowell, 1944).

Mossy fiber afferents are one of the two main input pathways to the cerebellum. They originate from the spinal cord and brain stem nuclei conveying proprioceptive and exteroceptive information, as well as copies of motor signals (efference copies, (Apps, Hawkes, 2009; Sommer, Wurtz, 2008). These axons ramify through the granular layer of the cortex, forming excitatory synapses with hundreds of Granule cells in large terminals called Mossy rosettes (Fig. 1.1 green), where information carried by a single Mossy fiber diverges extraordinarily (Ito, 2009).

Granule cells are the most numerous cells in the cerebellum, and the brain (Ito, 2009). Their soma is located in the granular layer, from where they project their axons to the Molecular layer and form T-shape branches called Parallel fibers (PF, Fig. 1.1 dark blue). These projections are densely packed and run longitudinally along the cerebellum, contacting hundreds of Purkinje cells (Eccles et al., 1967). It is estimated that each Granule cell receives information from around 5 different Mossy fibers. This way, different PFs carry different combinations of Mossy fiber input patterns, each carrying a distinct subset of contextual information (Huang et al., 2013). In addition to this, the individual effect of an active PF synapse on a Purkinje cell is neglectable. Only the summation of simultaneously active PFs can give origin to small, rapid depolarizing events called Simple Spikes (SS, Fig. 1.1 blue dot) (Barbour, 1993). Since Granule cells are thought to encode spatiotemporal representations of a determined body or environmental parameter, it is easy to imagine how different movements and contexts may lead to different SS representation patterns on different subsets of Purkinje cells.

Purkinje cells (PCs, Fig. 1.1 orange) are of special interest regarding the computations performed in the cerebellar cortex since they constitute its sole output pathway. They possess a large and dense dendritic tree in the molecular layer through which they contact tens of thousands of different PFs (Barbour, 1993; Napper, Harvey, 1988). These cells project their axons to the DCN in a projection area, forming GABAergic inhibitory synapses with several DCN neurons. Due to the overlap of these projection areas, each DCN neuron can be inhibited by multiple Purkinje cells from different parts of the cerebellum (Pantò et al., 2001). This suggests that different sets of PCs, representing diverse types information, contribute cooperatively to modulate the activity of DCN neurons. These will then modulate upper motor neurons, responsible for the organization and coordination of ipsilateral motor sequences in complex voluntary movements.

Purkinje cells possess another peculiar attribute, compared to other neurons in the brain: each one of them is surrounded by an axon that connects heavily to its dendritic arbor, called Climbing fibers (CF, Fig. 1.1 red) (Eccles et al., 1966). They originate from the inferior olivary neurons, in the contralateral brainstem, and are thought to carry instructive signals from sensory processing networks Ito (2001). These projections from the IO reach the cerebellar cortex and contact dozens of different PCs all the way to their dendritic tree, forming numerous synapses along the way Sugihara et al. (1996). Thus, when activated, these fibers lead to a powerful postsynaptic current in PCs, called Complex Spikes (CS, Fig. 1.1 red dot). These spikes strongly depolarize the cell, eliciting a pause in SS firing Eccles et al. (1966), believed to play a role in information processing within the cerebellar cortex (Marr, 1969; Albus, 1971; Ito, 1970). It is believed that CFs are able to regulate the weights of PF-PC synapses, consequently regulating the representations of information in each PC (Streng et al., 2018).

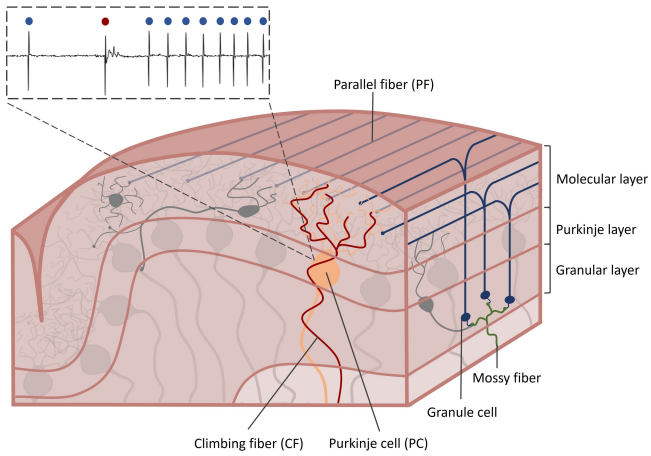

Figure 1.1: **Cerebellar cortex anatomy & Purkinje cells.** Cerebellar cross section representing the organization and the elements of the cerebellar cortex. Inputs to the cerebellar cortex arrive from Mossy (green) and Climbing (red) fibers. Mossy fiber inputs are distributed to Granule cells (dark blue) which, in turn, output to Purkinje cells (orange) through Parallel fibers. On the other hand, Climbing fiber output is directed to Purkinje cell soma and dendrites. Purkinje cell Simple (blue dot) and Complex (red dot) are the sole output of the cerebellar cortex.

1.2 The Cerebellum & motor outputs

Although the cerebellum is not required for movement initiation, it is crucial for the smoothness, speed, and precision of motor execution. Several bodies of work have clearly established this role of the cerebellum in motor control. First, damage to the cerebellum leads to ipsilateral limb movement and body posture disorders. Subjects with cerebellar dysfunctions exhibit an effective delay in movement initiation, abnormal movement termination (dysmetria), and clear decomposition of movements (movements are carried in a broken series of component motions), among others (Diener et al., 1992). Second, stimulation of the cerebellum evokes and regulates limb movements. Early studies demonstrated that electrical stimulation of the cerebellar cortex elicits characteristic postures and movements that vary systematically with the location of the stimulus. Chambers, Sprague (1955). In addition, more recent studies, using PC-specific optogenetic stimulation, have shown that PC activation is able to induce and perturb limb movements (Lee et al., 2015; Sarnaik, Raman, 2018). And third, cerebellar neurons are strongly modulated by movement. Single-unit recordings have shown changes in PC SS firing rates during a myriad of behaviors, such as reaching (Thach et al., 1992), smooth eye pursuit (Lisberger, Fuchs, 1978), locomotion (Sauerbrei et al., 2015), and licking (Bryant et al., 2010; Cao et al., 2012).

1.2.1 Purkinje cells in locomotion

Locomotion is a fundamental behavior in many different species. This type of behavior comprises several brain areas, as well as the spinal cord, that work collectively to regulate its initiation and coordination (for review, see Kiehn (2016)). The cerebellum seems to be essential for coordinated locomotion, where patients with cerebellar lesions (Morton, Bastian, 2007) and mouse mutant lines with Purkinje cell dysfunctions often display gait ataxia (Levin et al., 2006; Machado et al., 2015; Mullen et al., 1976; Walter et al., 2006).

In agreement with these observations, PC activity has been demonstrated to be closely related to step cycles and the overall speed of locomotion. Several studies have reported different rhythmic patterns of PC discharges time-locked to stride events during locomotion (as in Fig. 1.2 - A) (Armstrong, Edgley, 1984; Sarnaik, Raman, 2018; Sauerbrei et al., 2015; Udo et al., 1981), and baseline firing rate variation related to walking speeds (as in Fig. 1.2 - B) (Armstrong, Edgley, 1988; Muzzu et al., 2018).

More interestingly, PC activity during locomotion exhibits step-to-step variability (Sauerbrei et al., 2015). It has been suggested that this variability could be related to different limb variables within steps, such as speed, acceleration, relative position, etc. This points to the possibility that PCs make use of different step-related body information to modulate step cycles.

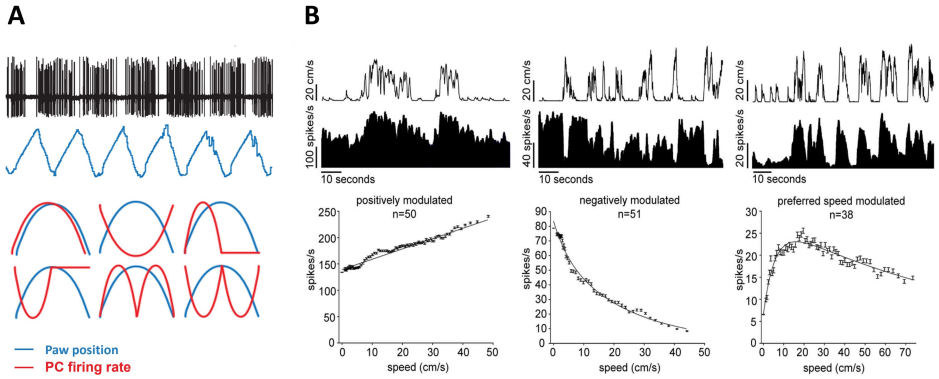

Figure 1.2: **Purkinje cell SS activity during locomotion. A)** Purkinje cell SS rhythmic activity (red) during stride cycles (blue), adapted from Sauerbrei et al. (2015). **B)** Different Purkinje cell SS activity related to locomotion speed, adapted from Muzzu et al. (2018)

1.2.2 Purkinje cells in licking

As locomotion, fluid licking is a vital behavior in almost all species. This behavior is highly stereotyped in rodents, characterized by sequences of fast lick events at a more or less constant rate, called lick bouts (Davis, Keehn, 1959). Similar to any other limb movement in locomotion, different muscle groups need to be rhythmically coordinated to perform a single lick, such as muscles involved in tongue protrusion and retraction, jaw opening and closing and swallowing.

Just as in other motor output coordination examples, the cerebellum also seems to be involved in licking. It has been shown that the cerebellar cortex plays a role in licking initiation and timing (Bryant et al., 2010; Tsutsumi et al., 2020). In agreement with these findings, several studies have demonstrated PC SS firing rate changes related to licking (Bryant et al., 2010; Cao et al., 2012). In their study, Bryant et al. (2010) describe two main types of modulation: Rhythmic and Non-rhythmic modulation. The first one describes cell responses that exhibit a periodical SS firing pattern related to the periodicity of licking. Conversely, the second one describes cell responses that are licking-related but do not possess the pattern above mentioned.

This suggests that PCs might encode different parameters related to the licking behavior, such as motor-related kinematics (possibly rhythmic responses) and state-dependent (possibly non-rhythmic responses).

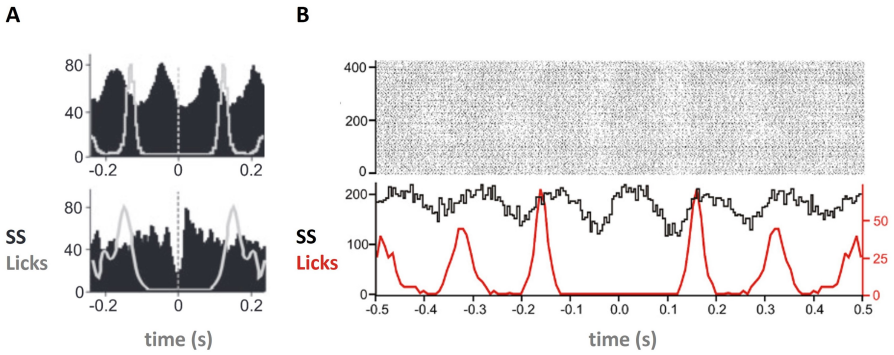

Figure 1.3: **Purkinje cell SS activity during licking. A)** Purkinje cell SS activity related to licking, revealing rhythmic **(top)** and non-rhythmic **(bottom)** firing patterns, adapted from Bryant et al. (2010). **B)** Rhythmic Purkinje cell SS activity correlated with licks distribution, adapted from Cao et al. (2012).

1.3 Aims

The work presented here is part of a larger project that aims to identify and to understand how single PCs in mice may encode different limb parameters to achieve coordinated locomotion. This dissertation, however, focuses on characterizing, in the same cells, a different modality of information: licking-related modulation.

More specifically, we first aim to identify the types of licking-related information being represented in the simple spike firing rate of individual Purkinje cells in mice. Second, once the modulations are quantified, we aim to relate this information with the cell's location within the cerebellum to test for functional organization.

2. Methods

For this project, we performed cell-attached recordings from cerebellar Purkinje cells during head-fixed locomotion in mice and analyzed the relation between licking behavior and neural data (Fig. 2.1). Mice were first subjected to a craniotomy and head post implant surgery. They were then trained for an associative task, where water is given as a reward for locomotion. This task was used to collect data from Purkinje cells during locomotion and, more relevant to this project, licking behavior during water reward consumption. Tongue position was tracked with DeepLabCut and used to identify lick events. These events were related with neural data, using time alignment analysis and Generalized Additive Models, to identify tongue-modulated cells. Cell positions were later estimated, matching stereotaxic coordinates with histological coordinates, and analyzed with the corresponding modulations. The details regarding each main step of the methodological pipeline are explained in this next chapter.

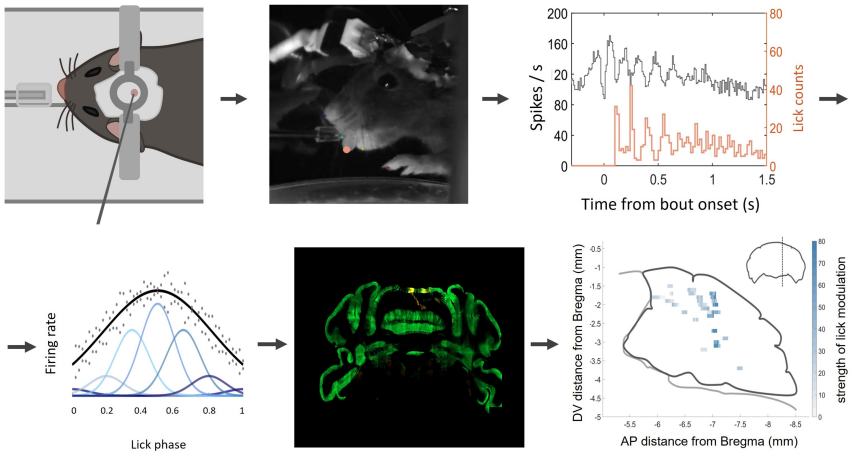

Figure 2.1: **Methodology overview.** Analysis pipeline conducted in this project. From left to right, single Purkinje cell recordings during head-fixed locomotion and licking, DLC tongue tracking, time alignment analysis, GAM analysis, cell location estimation, and cell population analysis.

2.1 Experimental setup

To perform cell-attached recordings from single Purkinje cells during locomotion, head movements have to be stabilized. For this, a custom-made head post is surgically bound to the skull (method described in section 2.3) and held by 2 metal clamps during experimental sessions (Fig. 2.2 - A). These metal clamps are positioned above a 2-belt wheel, where mice are allowed to locomote for a water reward (Fig. 2.2 - B). Water is delivered (5x10^{-3} mL / reward) via a water-spout positioned near the mouse's mouth (Fig. 2.2 - C).

Behavioral data is acquired through video recordings using 2 behavioral cameras: one facing the mouse's snout (licking camera, PointGrey Grasshopper, Teledyne FLIR, 120 fps, Fig. 2.2 - D) and another facing its lateral side (locomotion camera, Pike F-032 B/C, Allied Vision Technologies, 330 fps, Fig. 2.2 - E). Below the wheel, there is a mirror with a 45º angle reflecting the ventral side of the mouse to the locomotion camera (Fig. 2.2 - F).

Neural data is acquired with cell-attached glass electrodes that are advanced into the right side of the cerebellum, at a fixed angle, using a motorized micromanipulator located near the wheel (Fig. 2.2 - G).

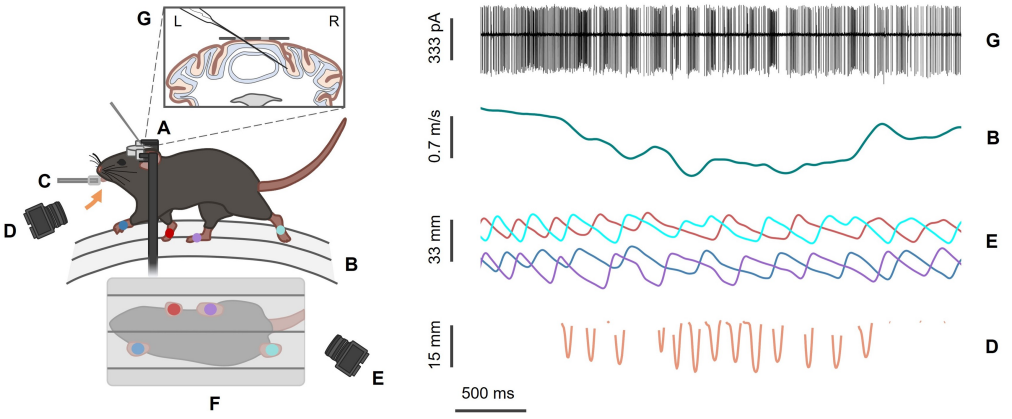

Figure 2.2: **Experimental data collection. A)** Metal head post fixed on the mouse's skull held by metal clamps. **B)** Setup wheel where mice are able to run, which triggers a water reward after a given distance. **C)** Lick spout where water rewards are delivered. **D)** Licking camera facing the mouse's snout to capture licking of the reward. **E)** Locomotion camera facing a mirror and the lateral side of the mouse to capture limb movements during locomotion. **F)** Locomotion mirror with 45º angle to capture the ventral side of the animal. **G)** Glass pipette used for electrophysiological recordings of Purkinje cells to record from the right side of the cerebellum.

2.2 Animals

Experiments were performed on 6 male adult ($\sim$ 2 month old) C57BL/6J mice (B6; mus musculus), housed in a temperature-controlled vivarium under a reversed 12:12h light/dark cycle with food and water ad libitum.

After surgery, mice were single housed with restricted access to water during the weekdays ($\sim$ 1mL / day) and allowed ad libitum access to water for 5 minutes before the weekend. Access to food was never restricted. Bodyweight was measured daily to guarantee that it was never under 85% of the weight pre-water restriction.

All procedures were carried out following the European Union Directive 86/609/EEC and approved by the Champalimaud Centre for the Unknown Ethics Committee and the Portuguese Direção Geral de Veterinária (Ref. No. 0421/000/000/2020).

2.3 Surgery

In every surgical session, mice are weighed and anesthetized with isoflurane (4% for induction and 0.5-1.5% for maintenance). They are placed in a stereotaxic frame (David Kopf Instruments, Tujunga, CA), which fixes the mice's heads and provides a continuous flow of air and isoflurane during surgeries. Both eyes are covered with an ophthalmic gel (Visidic gel, Bausch&Lomb) to prevent dryness, and body temperature is maintained around 34 ºC with a heating pad.

Initially, the scalp skin is removed by performing a small cut between the ears with surgical scissors, uncovering bregma and lambda. This area is then abundantly treated and cleaned with an iodine solution, saline solution, and sterile cotton swabs. To provide access to the brain area of interest, a 3 mm diameter craniotomy is performed using a biopsy punch, considering its relative position to lambda. This aperture is located below lambda, on the right side of the interparietal bone (Fig. 2.3).

Afterward, a 3 mm circular glass coverslip with 4 drilled holes is used to cover the exposed dura, glued to the skull with a quick bond glue (VetBond 3M, Fig. 2.3). These holes serve as electrode entrance points during electrophysiology recordings. For post-hoc estimation of the stereotaxic coordinates of the recordings, the three-dimensional coordinates for each hole, bregma, and lambda are measured using the stereotaxic frame coordinate system. Then, a custom-made metal head post is bound to the skull using dental cement (Super Bond - C&B, Fig. 2.3), and covered with a biocompatible silicon-based elastomer (Kwik-a cast, WPI), to prevent tissue dryness and debris deposition. Mice are fed a gel solu-

tion containing analgesic and antibiotics and allowed $\sim$ 3 days to recover before being water restricted.

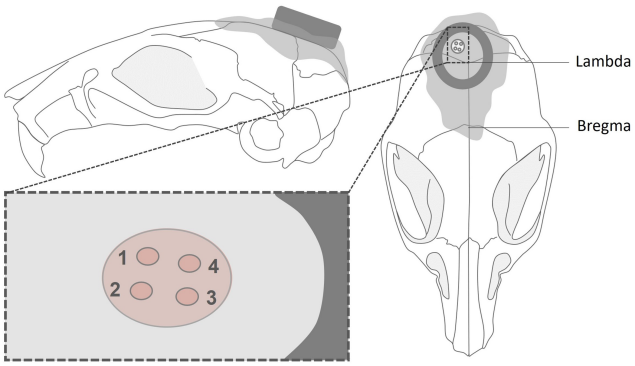

Figure 2.3: **Craniotomy and head post implant.** Illustration representing the positions of the cranial window and the head post relative to Bregma and Lambda in the mouse skull. During recording sessions, the cranial window holes exemplified here serve as entrance points for the glass electrodes.

2.4 Behavior

2.4.1 Behavioral task & training

After recovering from the surgical procedures, mice are trained to locomote head-fixed on our experimental wheel for water rewards during single trials of $\sim$ 30s. These trials are delimited by the control of a wheel brake, preventing the mouse from moving the wheel between trials. Each training set lasts for $\sim$ 5-15 days, where each daily session ends whenever the mouse reaches 1 mL of consumed water ($\sim$ 200 rewards).

In early training sessions, the reward is manually triggered every time the mouse initiates locomotor movements to reinforce the association between locomotion and reward. As soon as mice start to exhibit voluntary epochs of locomotion, an automatic delivery system based on traveled distance is used instead. This sys-

tem triggers reward delivery whenever mice reach a target distance within a 10 s window. It also continuously increases the target distance on each delivery (Δ = 0.5 cm), steadily increasing the number of strides needed between rewards. The initial distance and increments are adjusted in each session to optimize learning, based on the mouse's performance.

Whenever mice can maintain periods of locomotion of > 0.7-1 meter per reward interval, they are considered trained and ready for experiments.

2.4.2 Body features tracking

Tracking of behavioral features was performed post-hoc using DeepLabCut (version 2.1.8.2) (Mathis et al., 2018; Nath et al., 2019), an open-source algorithm that allows for markerless 2D or 3D pose estimation on video recordings, using deep neural networks trained with user input. More specifically, we labeled 25 frames, chosen with a k-means clustering algorithm, from 46 licking camera videos of different sessions and mice (then 95% was used for training). We used a ResNet-50-based neural network with default parameters for 5x10^5 training iterations. We validated with 1 number of shuffles and found that the test error was: 4.89 pixels to condition the X, Y coordinates for future analysis. This network was then used to analyze videos from all experimental sessions.

We trained the custom network to track 6 different markers in the licking camera behavioral videos: tongue, left and right front paws, nose, the lower part of the mouth, and waterspout (Fig. 2.4). However, for the work presented here, we only made use of the tongue marker.

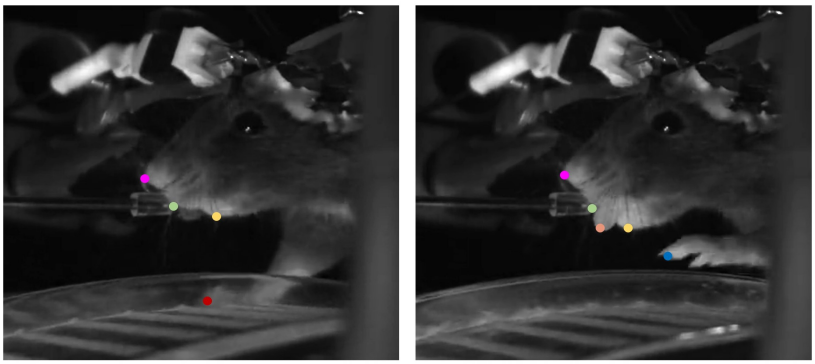

Figure 2.4: **DLC markers used for tracking licking behavior.** Representative frames of a video recorded with the licking camera illustrating the user-defined marker positions for DLC tracking: Front right paw (red), Front left paw (blue), the lower part of the mouth (yellow), tongue (orange), waterspout (green), and nose (magenta).

2.4.3 Lick and Lick bout identification

To identify lick events, we first transformed the two-dimensional image coordinates of the tongue tracking into tongue displacement (tongue displacement (mm) = $\sqrt{(x^2 + y^2)}$). This way, we can estimate the protrusion of the tongue during each lick. It is important to note that, for visualization purposes, tongue displacement was inverted to match the expected tongue protrusion).

Local maxima (licks) are identified using a Matlab built-in function (findpeaks, MinPeakProminence = 2% minimum value). Due to the fact that, in some cases, tracking failed during lick onset/offset, we choose to keep lick timings at the point of maximum displacement.

Sets of fast sequential licks (lick bouts) are identified using a custom-made algorithm that groups sequential licks with inter-lick intervals below 500 ms. Only lick bouts with a minimum of 5 licks are considered.

2.4.4 Licking behavior analysis

Statistical analysis was conducted using Matlab software. For the licking behavior analysis, we only took into account licks belonging to lick bouts.

The total lick and lick bout number distribution was done using bin sizes of 200 licks and 10 lick bouts, respectively. The average and standard deviation reported were calculated using built-in Matlab functions.

For the lick bout analysis, linear fitting was done with the median lick bout size (number of licks) and duration in each session, fixing the intercept at 0. The coefficient and statistics reported were given as output from Matlab's regress function.

The median inter-lick interval distribution was done using bin sizes of 8.75 ms. The average and standard deviation reported were calculated using built-in Matlab functions.

2.5 Neural data

2.5.1 Recording sessions

Cell-attached recordings on single-cells are performed using borosilicate glass electrodes (Warner Instruments), made with a vertical puller (Narishige PC 100), filled with saline solution (9% NaCl, resistance: $\sim$ 4 MΩ). We use a Multi-clamp 700B amplifier (Axon Instruments) in its voltage-clamp configuration, with a 2.5 V/nAp gain and low-pass Bessel filter with a 10 kHz cut-off frequency. The current offset between the interior and exterior of the electrode is always kept neutral. The output signal from the amplifier is digitized using a NI-DAQmx board, at a sampling rate of 25 kHz.

In every experimental session, the mouse is weighed, head-fixed to the setup, and the biocompatible silicon covering the cranial window is removed. The cranial window is properly cleaned, and the head post well filled with saline solution.

The electrodes are advanced into the cerebellum at a fixed angle, through one of the 4 coverslip holes using a precision controller (PatchStar Motorised Micromanipulator, Scientifica). Purkinje cells are identified based on their firing characteristics such as the sustained high-frequency Simple spikes (SS) firing rates and the presence of low-frequency Complex spikes (CS). The experimental session starts as soon as a good seal to the membrane and a high spike signal-to-noise ratio is achieved and ends whenever the animal ceases to exhibit voluntary locomotion or the cell is lost.

To approximate the cell position relative to the cranial window, the coordinate system of the micro-manipulator is used to measure the coordinates of the cell and all 4 holes of the cranial window, using the tip of the glass electrode.

Lastly, the cranial window is cleaned with saline solution and covered once again with biocompatible silicone for reuse in the following days. For each animal, experiments ended whenever the cranial window became opaque, due to healing processes, or broken, due to any sort of mechanical stress.

2.5.2 Neural data pre-processing

Due to the presence of both simple and complex spikes in the Purkinje cell recordings, spike sorting is performed in three main steps: data pre-processing, general spike identification, and SS/CS classification.

First, the raw recordings are high-pass filtered, removing low-frequency changes that may have occurred during movement, and filtered once more using a Wiener

filter, removing spurious high-frequency noise. Then, a custom threshold-based python algorithm is used to identify both types of spikes throughout trials, optimized for each session. To then distinguish CS from SS, we manually collect a sample of CS and train a custom Un'Eye neural network (Markanday et al., 2020) for each session. These networks are then used to classify the waveforms of CS throughout the corresponding sessions.

Due to the nature of Purkinje cell firing patterns, the SS firing rate was computed using Inter-Spike Intervals (ISIs). We assigned the inverse of the ISI to the sampled points between each pair of spikes, generating a step-like firing rate (Fig. 2.5).

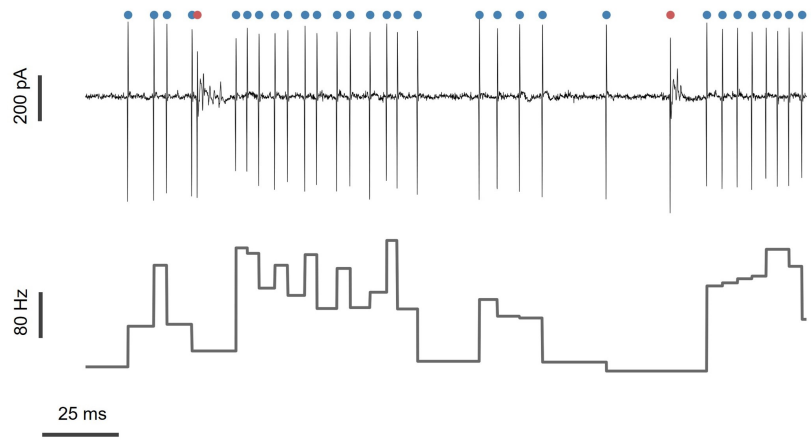

Figure 2.5: **SS/CS classification and SS firing rate estimation. Top:** Raw voltage-clamp recording with labeled simple and complex spikes (blue and red respectively). **Bottom:** Corresponding SS firing rate computed from the SS ISIs.

2.5.3 Neural data analysis

To identify tongue-modulated cells, we performed two sets of analyses: a time alignment analysis to describe the data as many other researchers have done in

the literature, and a more statistically formalized approach – Generalized Additive Models.

Time alignment analysis

Time alignment analysis is based on estimating correlations between independent variables using the timing of events as the aligning reference. In our case, we use this approach to assess the relationship between licking and the neural activity of our cell population.

To assess the different types of cell responses to licking, we extracted the SS and lick events inside a time window of -0.3 s to 1.5 s relative to lick bout onsets (first lick of a lick bout) in all cells. We then obtained the SS and lick histograms by using bin sizes of 10 and 20 ms, respectively. For interpretation purposes, the SS histogram is transformed into firing rate (firing rate (spikes/s) = $\frac{\frac{\text{nº spikes in bin}}{\text{nº lick bouts}}}{\text{bin size (s)}}$) and first licks are deducted from the distribution. Cell responses are characterized based on the relation between the SS firing rate and lick distribution, similar to Bryant et al. (2010).

For cell modulation classification, we calculate the Modulation Index as used in Sarnaik, Raman (2018) (MI (%) = $\frac{\text{max firing rate - min firing rate}}{\text{max firing rate + min firing rate}} \times 100$), a metric of modulation effect size for behavioral events. It is based on the assumption that if an event is not relevant to the cell's firing rate, the resulting firing rate average aligned to that event will be flat due to random jitter, and thus, the range between maximum and minimum values of the average will be close to 0. It also normalizes the average modulation amplitudes by the sum of its maximum and minimum values to facilitate comparisons between neurons with different baseline activities, enabling population quantitative analysis. For the calculation of firing rate averages, all computed firing rates were downsampled to 300 Hz to better match the sampling rate of the behavioral data.

Modulation assessment is based on a chosen MI threshold ($MI_{threshold}$ = 20%), in a 300 ms time window, using pre-identified modulated cells as reference. To identify licking-related cells, we first assess the cell MIs at the bout onset. Then, to identify the type of modulation (lick or bout modulation), we assess their MIs calculated by aligning instead to all the licks of each lick bout. We only analyzed sessions with more than 15 bouts, to reduce possible classification errors (n = 81 sessions)

Generalized Additive Models

One of the main drawbacks of time correlation analysis is its high sensitivity to correlations between independent variables, which greatly limits its interpretability. This limitation was observed in our datasets, where speed is correlated with lick bout onsets. So, to overcome this problem, we required a procedure that could identify the individual effect of licking in our cells.

Linear models are a common technique to quantify how a set of independent variables are individually and collectively related to a target variable, having the advantage of being easy to implement and interpret. If the model assumptions are met, they allow to remove the effects of some variables over another, as we intend with speed and lick bout onset. However, standard linear regression assumes the target variable is a linear function of the observed predictor variables.

For this reason, to identify the different contributions of speed, lick bout, and individual licks to the firing rate of the cell, we resorted to Generative Additive Models (GAMs). GAMs are a modeling technique with looser assumptions regarding linearity: it can approximate nonlinear relationships of individual predictor variables to a target variable, while also estimating their combined additive effect over the target variable (James et al., 2021). The GAM initializes by splitting each predic-

tor variable into a given number of basis functions, usually in the form of splines, throughout the variable's observed range (as exemplified in Fig. 2.6 - B). Each initial set of basis functions has a matching set of coefficients that define the amplitude of each spline, and at this stage, all of the function-coefficient pairs add up to a constant value over the variable range. Then, the model optimizes all basis coefficients from all variables simultaneously according to their estimated linear relationship to the target variable. Thus, the more a coefficient strays from its initial value, the higher its contribution to the target variable. And because each coefficient is independent of each other, inside the predictor variable, nonlinear relationships can be modeled as exemplified in Fig. 2.6 - C. After a GAM model has converged to an optimized solution, we can extract the isolated contribution of each predictor to the target variable through the calculation of its partial dependency, which is the aim of this approach: disentangle the speed and lick bout onset effects on the firing rate.

To implement the GAMs in our data, we pre-processed all variables to ensure continuity through time, avoiding data omissions, and to increase the interpretability of the model. For instance, to prepare the licking data, we use an approach already implemented by Sauerbrei et al. (2015) and transform the sequences of lick time events into continuous phase vectors suitable for our modeling. We build an array containing the normalized timings between sequential licks in a bout, ranging from 0 to 1, that corresponds to the inter-lick phase (Fig. 2.6 - A blue). This way, if there is a consistent contribution from every single lick on average, it will be captured within this phase. To distinguish the contributions between individual licks and the whole lick bout we build another phase array containing the lick indices relative to the first lick of each bout. We fix the number of licks to 10, ensuring all lick bouts are equally represented (Fig. 2.6 - A red). This way, if there is a contribution from the lick bout, independent from each individual lick, it will be captured within this array instead. All variables given to

the model are interpolated to match the same sampling rate of the locomotion behavioral camera at 330 Hz (Fig. 2.6 - A), following the procedures established in the lab for these data.

For the target variable, the model is set to predict the inverse of the firing rate (in other words, the ISIs) throughout the whole concatenated trials. ISIs are used since their distribution fits much better the family of exponential error distributions available for the GAMs. The best fitting distribution in our GAMs is the inverse gaussian, with the identity link function, which renders almost normal distributions of all models' residuals.

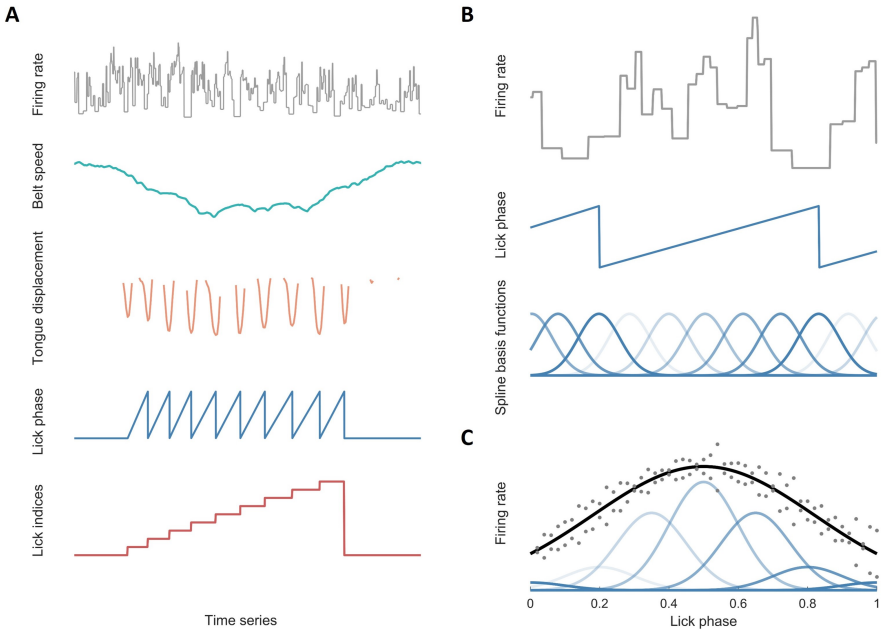

Figure 2.6: **GAMs input pre-processing and coefficient optimization. A)** Processed inputs used for GAM analysis: Firing rate (Gray) as the target variable, Belt speed (Green), Lick phase (Blue), and Lick indices (Red) as predictors. **B)** Demonstration of the Lick phase spline distribution **C)** Demonstration of the Lick phase GAM output with optimized coefficients for each spline.

GAM analysis was performed in R, using the MGCV package (Wood, 2011). We fit the GAM using the following pseudoformula: ISI $\sim$ s(belt speed) + s(lick indices) + s(lick phase), using a number of cubic splines equal to 30, 10, and 30, respectively. Sessions with low amounts of licking data were excluded by the model algorithm (total n = 78 out of 95 sessions).

Model predictions were transformed into firing rate by inverting the sum of the predicted ISI and the model's intercept (predicted firing rate (Hz) = $\frac{1}{\text{predicted ISI}} + \frac{1}{\text{model intercept}}$).

The model pseudo-R^2 is calculated using the following formula:

$$\text{pseudo-}R^2\ (\%) = \frac{\text{LL(null model) - LL(full model)}}{\text{LL(null model) - LL(saturated model)}} \times 100$$

The model deviance is calculated using the following formula:

$$\text{Deviance}\ (\%) = (1 - \frac{\text{LL(full model)}}{\text{LL(null model)}}) \times 100$$

For cell modulation classification, we start by transforming the output partial dependency (PD) of each variable into the corresponding firing rate (PD firing rate (Hz) = $\frac{1}{\text{partial dependency}} + \frac{1}{\text{model intercept}}$).The model intercept represents the overall cell's activity not explained by any of the analyzed variables (can be interpreted as baseline activity). Based on this, we calculate a GAM Modulation Index (GMI(%) = $\frac{\text{max PD firing rate - min PD firing rate}}{\text{baseline firing rate}} \times 100$), as an effect size metric for each variable contribution. Based on pre-identified modulated cells, we use a $\text{GMI}_{\text{threshold}}$ = 30% to identify the different types of modulation present in each cell.

2.6 Histology

2.6.1 Tissue pre-processing

At the end of all the experiments made in a mouse, the animal is fixed in the experimental setup, and a glass electrode is filled with a cell labeling solution (Vybrant™ Dil Cell-Labeling Solution, ThermoFisher) is inserted into each cranial window hole that was used during recordings. For each hole, the electrode is placed at the deepest coordinates recorded, and then slowly retrieved while ejecting its content with low positive pressure. Mice are then perfused transcardially with 4% paraformaldehyde and their brains extracted.

Brains are later sent into the histology platform, where they are cut in a vibratome, into coronal sections 50 µm thick, and stained for Purkinje cells (anti-calbindin primary antibody) and cell viability (DAPI marker). Brain sections are mounted on glass slides with a mowiol mounting medium and stored at 4ºC.

2.6.2 Tissue imaging

Tissue imaging was performed using a Zeiss AxioScan Z1, an automated wide-field slide scanner, equipped with Colibri 7 LED illumination and fluorescence filters. Brain sections were imaged with a Plan-Apochromat 20x/0.8 objective. A Colibri.7 LED provided the excitation lights of 385 nm, 475 nm, and 555 nm that we used to respectively excite DAPI, ALEXA-488, and Vybrant Dil. The three channels were sequentially acquired using a set of QBP 425 / 30+514 / 30+592 / 25+709 /100, BP 507-546, and BP 583-601 filters, based on the peak emission wavelengths (465 nm, 517 nm, 561 nm). The fluorescence signal was captured by a high-sensitivity monochromatic sCMOS camera (Hamamatsu Orca Flash 4.0 v2), with a pixel size of 6.5 x 6.5 µm, using the following exposure times: 10ms, 25ms, 10ms, respectively.

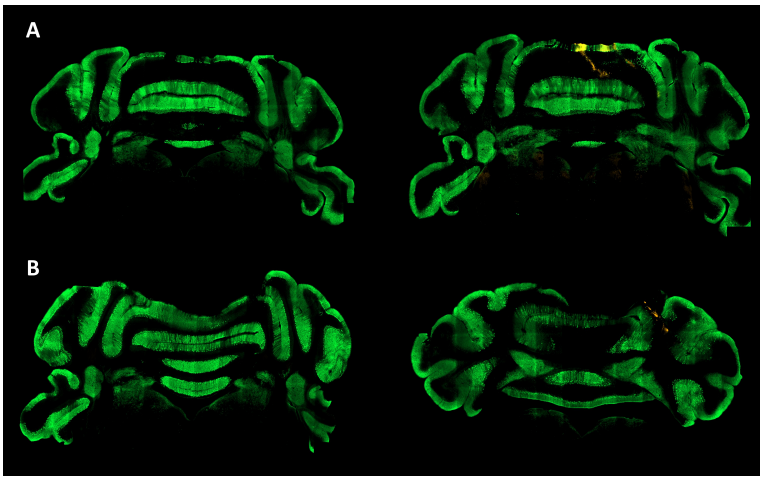

Figure 2.7: **Acquired brain images.** Brain section images stained for Purkinje cells (anti-Calbindin, Green) and Vybrant DiI (Dark yellow) for the path of the electrode, acquired using the Zeiss AxioScan.Z1 at 20x. **A)** Two brain sections of a representative animal with good histology, showing a slice far from the electrode path (**left**) and another one with two clear eletrode paths (**right**). **B)** Two brain sections from an animal with histological deformation, showing one electrode path **right**.

2.6.3 Cell location approximation & analysis

As for the preliminary results regarding cell distributions in the cerebellum, we approximate the cell coordinates recorded during the experimental sessions to the observed electrode paths labeled in histology. This process is done in three main steps: identification and stereotaxic coordinate approximation of electrode path, experimental and histological coordinate matching, and cell coordinate stereotaxic approximation.

For the electrode path identification, we start by stacking the acquired coronal brain section images in their respective order (anterior to posterior) for each mouse (as exemplified in Fig. 2.7). We observed that all brains exhibited, with varying severity, a deformation located in the medial dorsal region (as observable in Fig. 2.7). We attribute this deformation to the pressure inflicted by the cranial window, which pushed the cerebellar areas underneath. This nonlinear deformation prevents the use of current automatic image registration software to

match brain sections with a given reference atlas. For this reason, we opted for a manual estimation of the stereotaxic coordinates from the electrode path, using the Paxinos Atlas (Paxinos, Franklin, 2012) as the reference.

Manual stereotaxic coordinate estimation is done by first looking for the brain atlas section that best matched our histology brain sections (as exemplified in Fig. 2.7). Then, for each electrode path found in histology, we approximate the location of 2 different points in the atlas: electrode entrance point (the most anterior and dorsal point, as exemplified in Fig. 2.8 x1, y1, z1) and the electrode end point (the most posterior and ventral point, as exemplified in Fig. 2.8 x2, y2, z2). The coordinates of the estimated entrance points found in histology are compared with the cranial window surgical coordinates to match each electrode path with its corresponding cranial window hole. Due to lack of staining or damaged tissue, we were only able to identify 11 out of the 20 expected paths (containing 66 out of 95 cells recorded).

For cell stereotaxic coordinate approximation, we first start by calculating the euclidean distance of each electrode path found in histology (HD), using the approximate entrance and end points (as in Fig. 2.7). This way, we can match each hole's HD with its corresponding maximum experimental distance (ED), measured with the coordinate system of the micromanipulator (these should match as described in Section 2.6.1). Finally, cell stereotaxic coordinates are approximated by assuming that HD and ED are the same, since the electrode can only move in one direction inside the brain, and then substituting the location-to-endpoint distance ratio from ED to HD. Every estimated cell location was verified in histology by evaluating its position relative to a Purkinje cell layer.

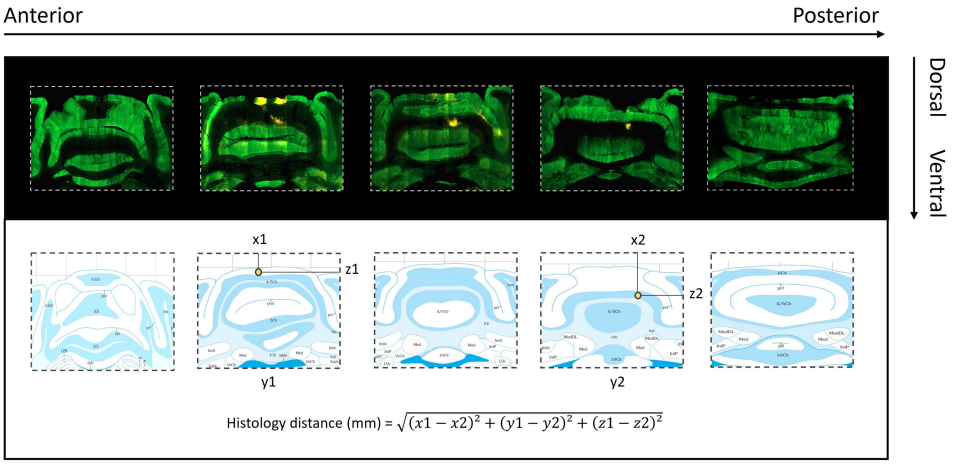

Figure 2.8: **Electrode path distance estimation.** Stereotaxic approximation for the entrance point (x1,y1,z1) and end point (x2,y2,z2) of the electrode path, using the Paxinos Atlas as reference. As described on the text, the histology distance is calculated using the euclidean distance formula.

For the distribution of cell modulations in space (seen in Fig. 7) we bin the 2D space across 2 different planes (DV-ML and DV-AP), using bin sizes of 0.1 mm for the DV and ML axis, and 0.05 mm for the AP axis. The different bin sizes are due to the fact that cells are less distributed along the AP axis, so a smaller bin size is used to contain fewer cells in each bin. Then, for each bin, we identify the cells inside and calculate the average MI values, based on the output from the GAM analysis.

3. Results

In this chapter, we present the results of the analysis described above, performed on behavioral and electrophysiological data from 95 experimental sessions, using 6 different mice, with the goal to identify tongue-modulated Purkinje cells and analyze their distribution in the 3D space.

3.1 Development of tongue tracking

To identify possible licking-related modulation, we first developed an approach to estimate the position of the tongue throughout each experimental session. For this, we used DeepLabCut (DLC), where we trained a custom deep neural network to perform 2D tracking of the tongue on our licking behavioral video recordings (Fig. 3.1 - A, as described in Section 2.4.2).

Tongue protrusions (licks) are identified by finding local maxima on a transformed output of the DLC coordinates (tongue displacement, as described in Section 2.4.3). Licks are then grouped in lick bouts based on the time interval between sequential licks (minimum of 5 licks with a maximum inter-lick interval of 500ms, Fig. 3.1 - B).

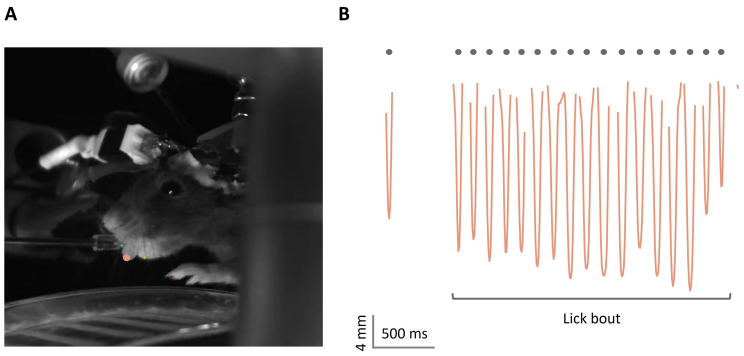

Figure 3.1: **DLC tongue tracking and lick identification. A)** Behavioral video frame with the tongue marker used for tracking (orange). **B)** Tongue displacement computed from DLC marker coordinates with lick timings identified (gray) at maximum tongue displacement, showing the corresponding lick bout.

3.2 Characterizing licking behavior

To gain insight into the licking behavior in our data set, we first looked at the distribution of the total number of licks and lick bouts per session (Fig. 3.2 - A & B). We observed an average of 922 ± 874 licks and 62 ± 49 lick bouts in each session. The variability in these distributions can be explained by either different task performances, which determines the number of rewards given, or by non-stereotypical licking behaviors, with intra- and inter-mice licking variability.

We started the analysis by addressing how stereotypical is the licking behavior of mice in our dataset. For this, we evaluated the linearity of the relation between the number of licks in a bout and its corresponding duration throughout our sessions by fitting a linear regression (Fig. 3.2 - C). Due to the absence of lick bouts, 5 sessions were excluded from the current analysis (n = 90 sessions).

We report an $r^2 = 0.959$ ($y=0.15x$, p-value < 0.001), indicating that the relation between lick bout size and duration (lick rate) is preserved across different sessions and mice. This also informs us that we should expect in our dataset an approximate inter-lick interval of 150 ms on average, given the slope of the linear regression. We confirmed this value by analyzing the median inter-lick intervals of each session, resulting in an average of 150 ± 13 ms (Fig. 3.2 - D).

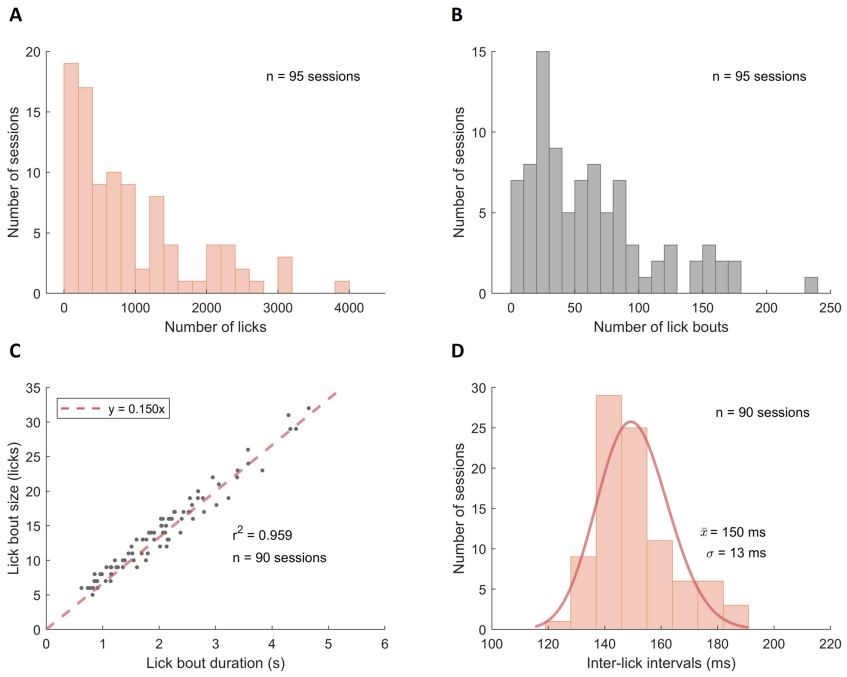

Figure 3.2: **Licking behavior summary. A)** Distribution of the total number of licks across all sessions. **B)** Distribution of the total number of lick bouts across all sessions **C)** Linearity between the median lick bout size and duration across different sessions. **D)** Distribution of the median inter-lick intervals across all sessions.

3.3 Estimating licking-related SS modulation

3.3.1 Identification of cell responses to licking

To look for evidence of licking-related responses, we first start by analyzing the correlation between SS and licking in a random subsample of cells. For this, we compare the distribution of SS and lick timings around lick bout onsets, in a given time window (Fig. 3.3 - A-C, described in Section 2.5.3 - Time alignment analysis).

We identify three major types of representative responses: Lick Modulation (LM), Bout Modulation (B), and Non-Modulated (NM). LM cells are characterized by the

presence of periodical patterns of SS, correlated with the lick distribution along the lick bout (similar to rhythmic firing units described in Bryant et al. (2010), Fig. 3.3 - A). BM cells, instead, display an overall pattern of SS which does not correlate with the rhythmicity of licking (similar to non-rhythmic firing units described in Bryant et al. (2010), Fig. 3.3 - B). Finally, NM cells are those that do not show any type of activity related to licking, with a homogenous SS distribution (Fig. 3.3 - C).

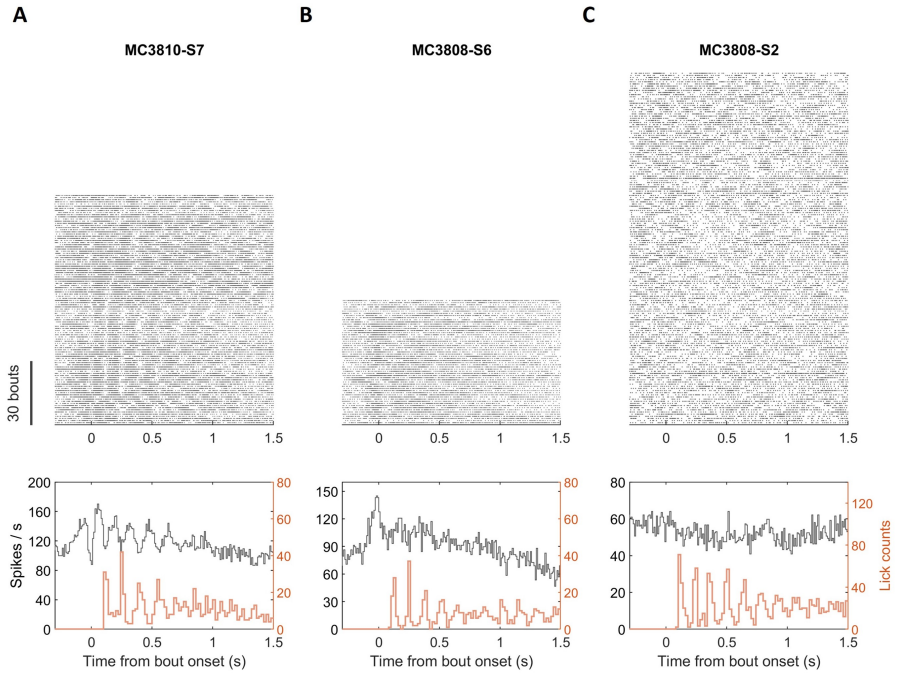

Figure 3.3: **SS and Lick time correlations.** SS rasters (**top**) and SS + Lick histogram (**bottom**) aligned to lick bout onset. Bin size: SS - 10ms, Lick - 20ms. **A)** MC3810 - S7 Lick Modulated cell with a rhythmic SS pattern correlated with lick histogram. **B)** MC3808 - S6 Bout modulated cell with SS increase at bout onset and no correlation with lick histogram. **C)** MC3808 - S2 Not-modulated cell with no response to licking.

3.3.2 Classification of time-aligned licking modulation

We then sought to identify modulated cells within the population and classify them based on the previously described responses. For this, we start by using a simple metric that serves as a proxy for the strength of modulation - the Modulation Index (MI (%) = $\frac{\text{max - min}}{\text{max + min}} \times 100$). This metric is calculated considering the amplitude of the average firing rate aligned to a given event. The more a cell is modulated by the event, the closer to 1 its MI will be, thus we can identify modulated cells using a simple threshold ($MI_{threshold}$ = 20%). Sessions with less than 15 lick bouts were excluded from the following analysis (n = 81 sessions).

To identify modulated cells (either lick or bout modulation), we start by assessing the cell MIs at bout onset (Fig. 3.4 - A). Based on the chosen threshold, we determine that around 73% of cells in our population exhibit lick-related modulations (Fig. 3.4 - B). Next, we try to distinguish between LM and BM cells, within the modulated subpopulation (n = 59 sessions), by assessing the cell MIs when aligning to every lick (Fig. 3.4 - C). Based on the same chosen threshold, we report that in the overall population, around 58% of the cells exhibit bout modulation (BM cells), while 15% are lick modulated (LM cells) (Fig. 3.4 - D).

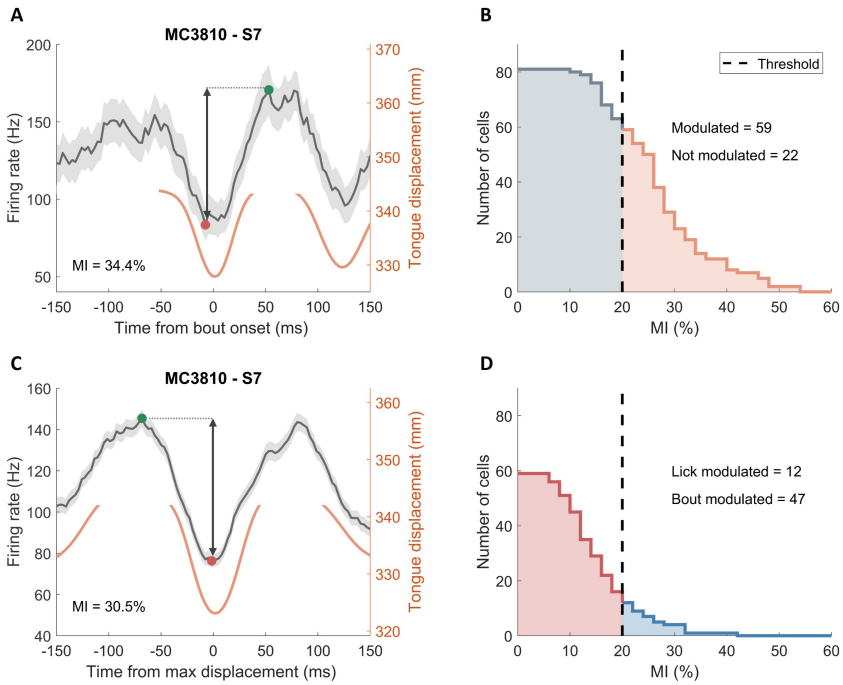

Figure 3.4: **Modulation Index and classification of cell population.** The green and red points correspond to the maximum and minimum values used to calculate the MI. **A)** Average firing rate ± 2 SEM (gray) aligned to lick bout onset for MC3810 - S7, with tongue displacement (orange). **B)** Bout onset aligned MI population values with 59 cells (orange) out of 81 being above the $MI_{threshold}$ **C)** Average firing rate ± 2 SEM (gray) aligned to single licks for MC3810 - S7, with tongue displacement (orange). **D)** Lick aligned MI population values from the population of lick bout modulated cells, with 47 cells (red) being below the $MI_{threshold}$ (only Lick Bout modulated) and 12 cells (blue) being above the $MI_{threshold}$ (Single Lick Modulated), out of 59.

However, one of the disadvantages of time alignment analysis is that it cannot separate the effects of any pair of correlated variables to the firing rate. In our data set, we identified a major confounding correlation within lick bout onsets and wheel speed: in most cases, mice stopped their locomotion right before starting the licking behavior. In addition, and as reported by some studies (Armstrong, Edgley, 1988; Muzzu et al., 2018) our recordings show that overall locomotion speed also modulates SS activity in Purkinje cells. Therefore, this raises the concern whether most of the cell responses observed at the lick bout onset, at-

tributed to bout modulation using the MI method, can be equally explained by the correlated speed variation (Fig. 3.5).

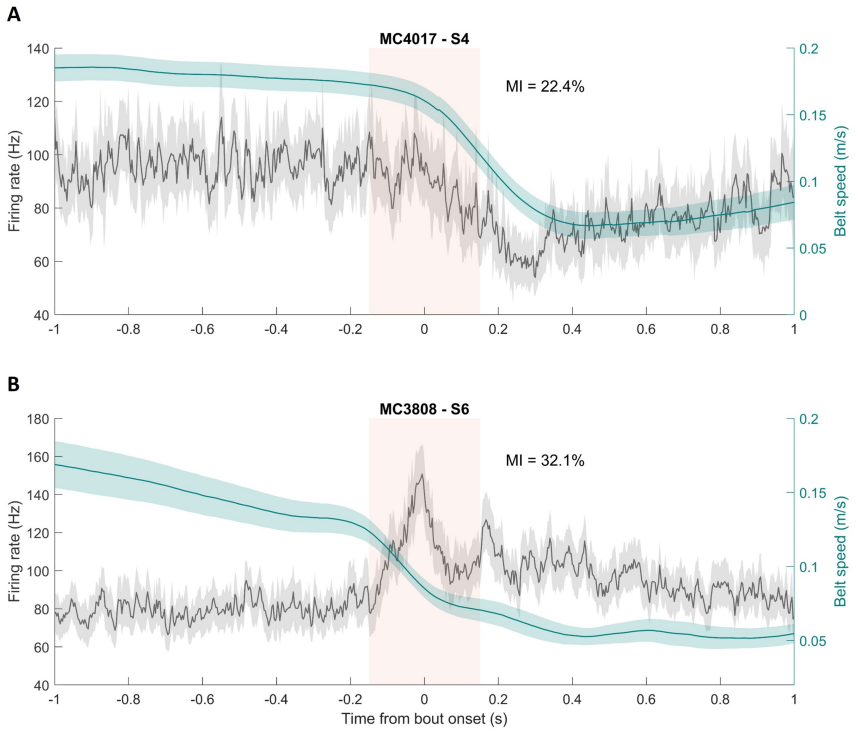

Figure 3.5: **Correlation between locomotion speed and with lick bout onset.** The shaded area corresponds to the time interval used to calculate the cell's MI at lick bout onset. **A)** MC4017 S4 average firing rate ± 2 SEM (gray) and belt speed ± 2 SEM (green) aligned to lick bout onset, illustrating a possible linear correlation between speed and firing rate. **B)** MC3808 S6 average firing rate ± 2 SEM (gray) and belt speed ± 2 SEM (green) aligned to lick bout onset, illustrating a possible nonlinear anti-correlation between speed and firing rate.

3.3.3 Classifying behavioral modulation through GAMs

To overcome the obstacle introduced by the confounding effect of locomotor speed correlation with licking, we sought a method that was able to disentangle the individual contributions of different variables to the firing rate variability throughout time. For this, we used Generalized Additive Models (GAMs), a modeling technique similar to Generalized Linear Models, with the ability to capture both the linear and non-linear effects of different predictive variables, through the optimization of multiple smooth functions.

In order to extract the individual contributions of speed, single licks, and lick bout, we feed the model three different variables to predict the firing rate variability: Belt speed, Lick phase, and Lick indices (Fig. 3.6, described in Section 2.5.3 - Generalized Additive Models). Sessions with low amounts of data were excluded by the model's algorithm (total n analyzed = 78).

To demonstrate how the model can disentangle the individual contributions of the predictor variables, we present the output model for the MC3808 - S6 session (Fig. 3.6 - A) where speed correlation to the bout onset was previously observed (Fig. 3.5 bottom). In this case, we want to identify whether the observed firing rate was due to lick bout onset, speed variation, or a combination of both. First, we checked whether the selection of model parameters, such as the choice of error distribution and link function, approaches the required assumption of normality of residuals for our data. As seen in Fig. 3.6 - A top, the output of the model with the best model parameters seems to be able to capture the observed trend in the raw firing rate. Then, by isolating the partial contributions that each variable has on the model (of speed, lick indices, and lick phase, Fig. 3.6 - A bottom), we can observe how both belt speed and lick bout onset add up to most of the model amplitude, while lick phase exhibits almost no contribution.

To assess the goodness of fit and the explanatory power of the models, we calculated the pseudo-R^2 and the percentage of deviance explained, respectively. Models that are considered really well fit have a pseudo-R^2 between 0.2 and 0.4 (McFadden, 1977). However, most of the models lie within the 0 to 0.1 range (Fig. 3.6 - B). Similarly, the percentage of deviance explained is also low, ranging from 0 to 30%. One possible explanation may be that the variables used for the model are not enough to explain all the firing rate variability.

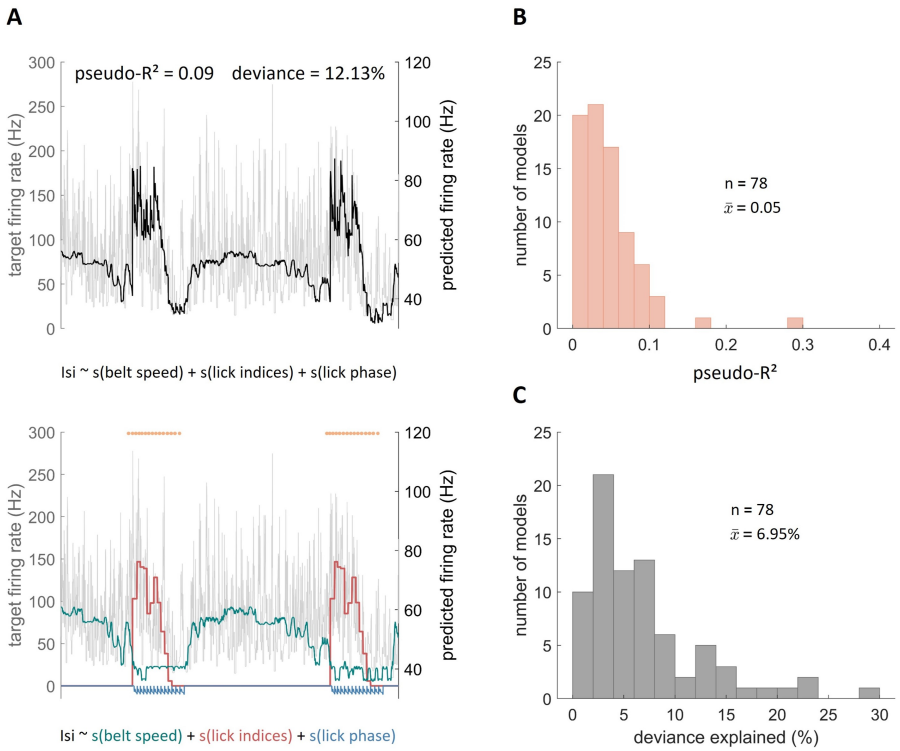

Figure 3.6: **GAM firing rate prediction and explained variability. A) Top**: Time window displaying the real firing rate of MC3808 - S6 (light gray) and predicted firing rate by GAM using belt speed, lick phases, and lick indices (black). **Bottom**: The same time window showing individual contributions from belt speed (green), lick phases (blue), and lick indices (red). Lick events are identified as orange circles **B)** Distribution of pseudo-R^2 values from all models. **C)** Distribution of the percentage of deviance explained from all models

Then, to quantify the different contributions from all three variables to each cell, we evaluated the model's partial dependencies. Partial dependencies can be interpreted as how the target variable, in this case, firing rate, changes along with the range of one predictor variable (i.e. lick phase) while the others are set to a fixed value (i.e speed and lick indices). In the absence of modulation, the partial dependency will be continuously flat across the whole range of the predictor variable, close to baseline values.

We can now observe how MC4017 - S4, a cell previously classified as BM (see Fig. 3.5), is mostly modulated by speed, with negligible contributions from individual lick and lick bout modulation (Fig. 3.7 - A). On the other hand, as seen in the previous figure, we now identify that MC3808 - S6, besides being modulated by speed, is in fact, also modulated by the lick bout onset (Fig. 3.7 - B, see also Fig. 3.5). And finally, we also present MC3810 - S7, a cell previously identified as LM, as an example of how lick modulation is still being captured by the lick phase partial dependency (Fig. 3.7 - C).

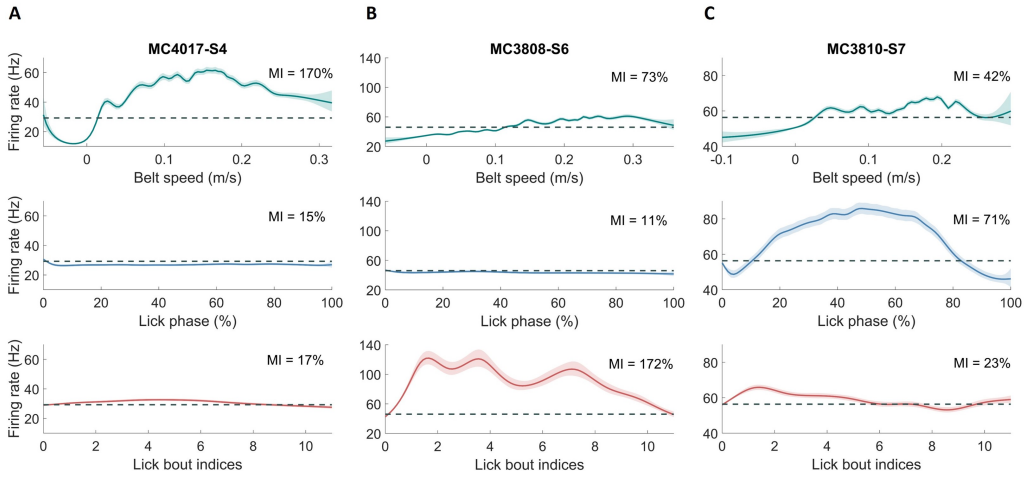

Figure 3.7: **GAM partial dependencies.** Model partial dependencies for three example cells: Belt speed (green), Lick phases (blue), and Lick indices (red). The dashed line represents each cell's baseline activity (extracted from the model's intercept value). **A)** Partial dependencies of MC4017 - S4, classified as a SM cell. **B)** Partial dependencies of MC3808 - S6, classified as a SM + BM cell. **C)** Partial dependencies of MC3810 - S7, classified as a SM + LM cell.

Thus, we can explore this method to identify modulated cells using another effect size metric based on the partial dependency output of the GAMs: the GAM Modulation Index (GMI (%) = $\frac{\text{max - min}}{\text{baseline}}$). Based on pre-identified modulated cells, we chose a GMI threshold of 30%. We determined that 99% of the cells exhibited speed modulation (Fig. 3.8 - A), showing once again how important it is to take into account this variable. We also determined that 42% of the cells are modulated by the lick bout (Fig. 3.8 - B), while 40% are lick modulated (Fig. 3.8 - C). Moreover, we can also assess the different combinations of simultaneous modulations. We identified that $\sim$ 15% of the cells exhibit the three types of modulation (SM + BM + LM), 27% of the cells are modulated by speed and the lick bout (SM + BM), $\sim$ 23% are modulated by speed and individual licks (SM + LM), and finally, $\sim$1% of the cells being modulated specifically by individual licks (LM) (Fig. 3.8 - D).

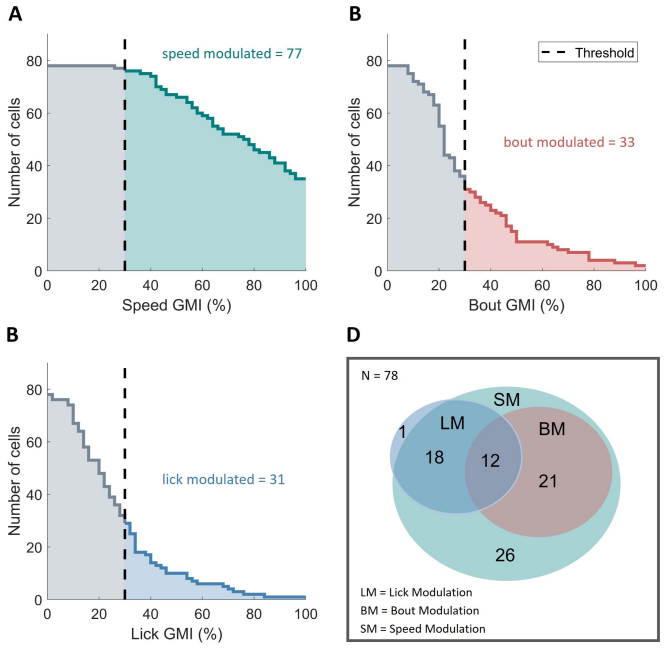

Figure 3.8: **GAM Modulation Index population analysis. A)** Speed GMI population values with 99% of the cells being above the chosen $GMI_{threshold}$. **B)** Lick bout GMI population values with 42% of the cells being above the chosen $GMI_{threshold}$. **C)** Single lick GMI population values with 40% of the cells being above the chosen $GMI_{threshold}$. **D)** Venn diagram with the number of cells that share different types of modulation.

A direct comparison between the two methods (MI and GMI) is shown in Figure 3.9, where we compare the number of cells for each type of modulation (NM - not modulated, SM - speed modulated, BM - bout modulated, LM - lick modulated) identified by each method. We first observe that the number of NM cells has decreased to none when using GAMs. This can be explained by the fact that in GAMs we introduced the variable belt speed, enabling the assessment of speed modulation, whereas in the time analysis method we cannot. Then, there is an observable difference in the number of BM and LM cells between methods, which can be explained by the fact that speed modulation is now taken into account, possibly decreasing false positives in BM cells and decreasing false negatives in LM cells.

Type of modulation	Nº of cells MI	Nº of cells GMI
NM	22 (27%)	0 (0%)
SM	---	77 (99%)
LM	47 (58%)	31 (40%)
BM	12 (15%)	33 (42%)
Total analyzed	81	78

Figure 3.9: **Population analysis based on MI and GMI values.** SM - speed modulation (green), BM - lick bout modulation (red), LM - lick modulation (blue). Corresponding number and percentage of identified cells exhibiting each type of modulation, based on MI and GMI values.

3.4 Anatomical distribution of modulated cells

In order to assess the presence of a possible relation between the cell modulation and its position within the cerebellum, we first coarsely estimate the position of each recorded Purkinje cell. This estimation is done by approximating the experimental session coordinates to the observed histological coordinates (described in Section 2.6.3). We were only able to approximate the positions of 66 cells, due to a lack of histological or experimental data (66 out of 95 recorded sessions).

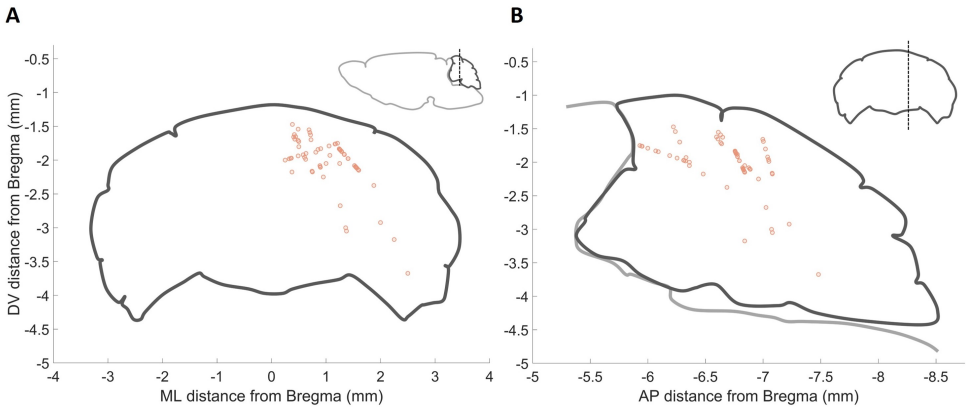

Figure 3.10: **Approximate anatomical locations of recorded Purkinje cells. A)** Coronal view of the cerebellum with the estimated cell DV-ML coordinates relative to Bregma. **B)** Sagittal view of the cerebellum with the estimated cell DV-AP coordinates relative to Bregma.

To assess whether there is an observable relation between cell locations and their modulation, we identify cells that share similar coordinates across the 2 different planes and assess the distribution of the average GMI values for each cluster. For this, we bin the 2D spaces in bin sizes of 0.1 mm, for the DV and ML axis, and 0.05 mm, for the DV axis, and calculate the average GMI for the three types of modulation analyzed (speed, lick, and bout modulation, as described in Section 2.6.3).

In the absence of any relation, we expect a uniform distribution of GMI values across both planes. Our preliminary results suggest a possible relation between the cell's AP coordinates and the average lick and speed GMI value. Cells within a -6.9 to -7.2 mm AP distance from Bregma seem to display higher lick and speed modulations than other cells (Fig. 9 - B & F). On the other hand, no other apparent relation seems to exist between other coordinate axes and modulation values (Fig. 9 - A, C, D & E).

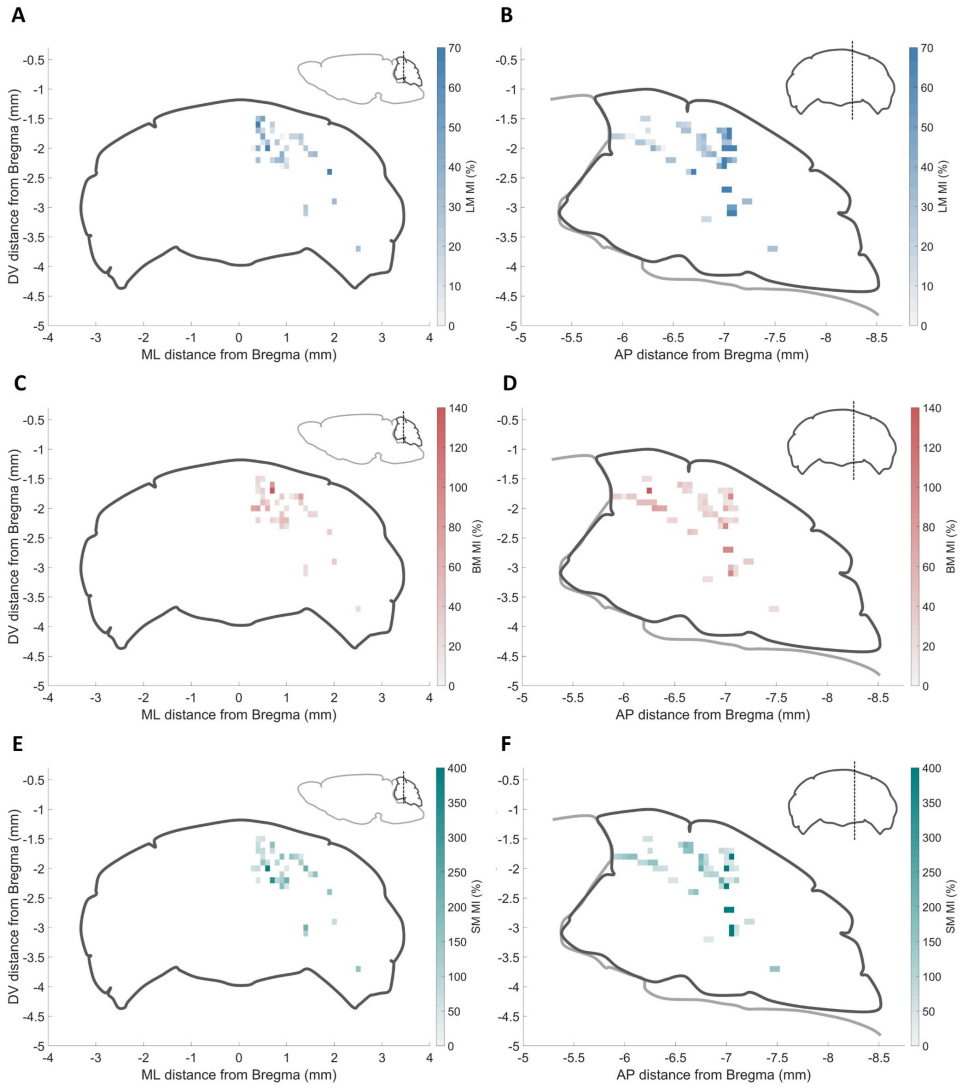

Figure 3.11: **Anatomical distribution of Purkinje cell modulation. Left row:** Coronal view of the cerebellum. **Right row:** Sagittal view of the cerebellum. **A-B)** Distribution of the average GMI for lick modulation. **C-D)** Distribution of the average GMI for lick bout modulation. **E-F)** Distribution of the average GMI for speed modulation. Bin sizes: 0.1mm, for the DV and ML axes, and 0.05mm for the AP axis.

4. Discussion

In this project we first aimed to identify and quantify licking-related modulation in mice Purkinje cell single units during a locomotion task, and second, to test for functional organization of the cells within the cerebellum.

4.1 Types of licking-related modulation

Consistent with the observations of Bryant et al. (2010), we identified two types of licking-related modulation: rhythmic and non-rhythmic modulation. The former is characterized by correlated SS firing with individual licks, while the latter is only correlated with the lick bout onset.

We can use these firing patterns to broadly speculate about the type of information being represented, for example: rhythmic firing patterns possibly encode combinations of different single-lick-related information (Lick Modulated), such as motor-driven kinematic properties of the tongue like position, speed, acceleration, or sensory-driven touch of the tongue to the water spout or water. Bryant et al. (2010) and Cao et al. (2012) also demonstrated that PCs may encode the relative timing between licks in their firing rates. This suggests that Lick Modulated (LM) cells may contribute largely to the coordination of the licking behavior, modulating/reporting licking parameters to achieve the stereotypic behavior rapidly and smoothly.

On the other hand, non-rhythmic SS firing patterns might encode either motor-driven information or more abstract licking-related information (Bout Modulated). It is unknown whether Bout Modulated (BM) cells respond to lick bout onset due to the fact that they evoke lick initiation (Tsutsumi et al., 2020) or are reporting lick bout initiation to inhibit other types of behaviors. They can also be representing the presence/absence of the water reward during the lick bout, as a sort of reward

prediction error (Heffley, Hull, 2019; Wagner et al., 2017). This nonlinear modulation type suggests that BM cells might contribute to the overall behavior of the animal, modulating/reporting lick bout parameters that reflect the current/future state of the animal.

However, to extract the answer to these questions, a more in-depth analysis of cell responses within each category would be necessary and it is important to note that this was not the goal of this dissertation. Thus, we only sought to identify and quantify the licking-related modulations in our cell population.

4.2 Modulation identification & quantification

As in previous studies, we employed time alignment analysis to quantify licking-related modulation on our neurons. By using the modulation index metric of Sarnaik, Raman (2018), we identified that the majority of our cell population exhibited licking-related modulation (73%, n = 59 cells), the majority being bout modulated (58%, n = 47 cells). These results suggest that, in the recorded areas, the somatomotor information may be less representative than expected. However, this is not in agreement with Bryant et al. (2010) observations, which show that rhythmic modulations were more prevalent in his recordings, nor with the abundant literature demonstrating direct links between PCs and kinematic representations (Popa et al., 2018).

To explain this disagreement, it is worth noting some strong caveats of the time-aligned analysis. First, the modulation index metric is biased due to its normalization formula. High firing rate modulations can be masked out if they are divided by a high baseline firing rate. Conversely, small modulations are accentuated in low baseline firing rate cells. This increases the chances of wrongly identifying the modulation of cells (both type II and I errors, respectively).

Second, this analysis does not provide unambiguous methods to identify significant modulations for our high-dimensional data. As our experimental design was optimized for locomotor behavior, we do not have a true measure of baseline activity to compare with moments of licking (the animal was moving throughout the recording session). Thus, we could not simply evaluate the excursions of firing rate outside an average baseline value as a proxy for modulation (as in Bryant et al. (2010)), because any baseline we define would shift depending on the locomotion. Consequently, a simple threshold of firing rate would also fail to discriminate noisy signals or locomotion modulation from significant licking modulation.

We also identified a significant number of recording sessions where lick bout onsets were strongly correlated with locomotion speed variation, as some mice either reduced or completely stopped locomotion to initiate the licking behavior. This raises the question whether the modulation index values estimated at lick bout onsets could be just a manifestation of speed modulation, a very prevalent modulation that many other studies have reported (Armstrong, Edgley, 1988; Sarnaik, Raman, 2018).

To overcome these issues, most previous studies implemented behavioral paradigms that isolate the effect of licking from other movement confounders, for example, by keeping the animal still during licking (Bryant et al., 2010; Cao et al., 2012). However, this also restrains our capacity to study the interactions between different sensory-motor information in a single Purkinje cell, the main objective of the project.

So, instead of studying the isolated effects of each behavioral modality, we used GAMs to extract the individual and combined relationships between them that explained the firing rate of the cell. With these models, we can take into account

speed modulation to correctly assess licking-related modulation. Compared to the results from the time-alignment method, the GAMs were more in agreement with previous studies.

First, speed modulation was present in almost all of our cells (77 out of 78 cells). Muzzu et al. (2018) reported that around 43% of their Purkinje cells (n=300) were tuned for speed modulation and that 53% were modulated by the phase cycle of paws during locomotion. Since we are not considering individual limb modulation, it is likely that cells possessing this modulation would express some speed modulation instead, given that locomotion speed is a direct consequence of limb movement. Therefore, we expect that by including the phase cycles of all 4 paws, the number of Speed Modulated (SM) cells would decrease, having some of the cells being attributed to paw modulation instead, getting closer to Muzzu et al. (2018) results.

Second, both types of licking-related cells are now equally represented in our population (33 cells for BM and 31 cells for LM, out of 78). This big change of proportions can be attributed to the high representation of speed modulation, which most likely confounded the output from the time-alignment method. The percentage of rhythmic firing PCs (LM cells) is now closer to what Bryant et al. (2010) have reported (24 out of 52). However, they reported a percentage of non-rhythmic cells (BM cells) far lesser than ours (8 out of 52). This difference might be explained by how time alignment analysis was conducted. In their study, the authors did not consider lick bout onsets, as we did. This way, small lick bout-related responses might have been hidden by the cell's overall baseline activity during licking.

Nevertheless, some caution must be present on the interpretation of our GAMs results. Since GAMs rely heavily on the quantity and combination of different pre-

dictor variables fed into the model, and our models had a very low explanatory power, we cannot guarantee that the measured effects of licking and locomotion speed would remain the same once more behavioral variables are taken into consideration, especially if they are highly correlated to each other. One already mentioned example would be the direct causal relationship between locomotion speed and individual limb modulations. Despite this lack of broad generalization in our current models, the relative relationship between licking and locomotion we found in this work should remain consistent, as these two behavioral modalities do not share related motor outputs. The optimal scenario, and current work in my research team, is to include all the available variables at our disposal to let the algorithm shrink the non-informative ones and optimize the functional representation of those more related to the firing rate of the cell.

With the GAM results, we were able to identify groups of cells that share different combinations of modulation simultaneously, such as: speed + single lick, speed + lick bout, and speed + single lick + lick bout modulations. As expected from their high number of shared inputs, our preliminary results show that the majority of our single cell population is encoding different modalities of information, in our case representing both locomotion and licking-related parameters simultaneously.

Our results are in agreement with recent bodies of work that suggest some neuronal ensembles might actually encode high-dimensional representations of body parts and behave differently in different contexts, a property termed mixed selectivity (Fusi et al., 2016; Mante et al., 2013; Meister et al., 2013; Rigotti et al., 2013) . Recent theoretical work has demonstrated that high-dimensional information, contained in individual units within a population, may be the optimal computational framework for parameter and context estimation (Johnston et al., 2020). Due to the vast amount and diversity of information being sent to the

cerebellar cortex via Granule cells, PCs seem to be perfect candidates as high-dimensional information integrators used in mixed-selectivity-like computations. Thus, we have reasons to believe that single PCs may be tuned to contain different body part representations, each expressed differently, which can then be used by DCN neurons to extract whole-body information in different states and contexts and provide the optimal relative output.

4.3 Purkinje cell modulation across the cerebellum

By examining the distribution of cells and their corresponding modulation values within the cerebellum, our preliminary results suggest a non-random pattern of higher speed and lick modulation in each set of coordinates along the sagittal plane. All other distributions did not exhibit a clear clustering of GMI values, instead, they looked random and uniformly distributed. This can point to the hypothesis that there is a nonlinear relation between Bregma distance and the effect speed and licking have on a given PC. Interestingly, only Speed and Lick modulated cells exhibited this pattern since they are the ones we most associate with direct sensory-motor information. Possibly, the rules of organization are different to cells encoding information beyond direct sensory-motor properties, such as Bout Modulated cells. Although highly speculative, a possible explanation for this tendency that could be tested in the future is that these cells, carrying more abstract types of information, can be more evenly distributed throughout the cerebellum to cooperatively modulate sensory-motor clusters directly involved in all kinds of behaviors.

If this is true, a possible mechanism for whole-body and contextual information integration is the existence of sensory-motor clusters specific to a given body part (as described by Snider, Stowell (1944)) being directly modulated by cells that represent high-order information, such as task performance, state of behavior, overall body activity, etc.

4.4 Mixed-selectivity for licking & locomotion

Even within the framework of mixed selectivity, what is the relevance of having single PCs tuned to represent such different modalities of information simultaneously, such as licking and locomotion behaviors?

First, the obvious example of the existence of coordination between these two behaviors is within the specific task here presented. When water was present, mice reduced their locomotion speed to initiate licking, optimizing the energy spent during the task, according to its priority. Highlighting the need to coordinate these two different behaviors to achieve optimal task performance. Second, even though we have not tested for that in this dissertation, preliminary results in the lab point to the fact that a big part of locomotion modulation in these cells might also be explained by multiple paw modulation. This can be linked to multiple natural behaviors of rodents, where these body parts function cooperatively, such as in the stereotypical feeding or grooming behavior. Here, the movements of the tongue must be somewhat coordinated with the relative position and movements of the paws to achieve a smooth and efficient motor output.

Thus, it is not surprising that the cerebellum contains the relative information of these two different behaviors within its circuit. It might employ a subset of Purkinje cells to represent sensory-motor states of body parts together with another subset that is specific to each context and task, to be read and decoded downstream and modulate behavior accordingly.

4.5 Project outlook

In the future, it would be interesting to further investigate the types of information being represented in each licking-related modulation. For example, in lick modulation, we can include the different kinematic variables of the tongue to identify

possible motor-related modulations. We can also take into account the moments the tongue touched the water spout to distinguish between motor and sensory information. For bout modulation, we can use the relative timing of reward delivery to assess whether it is more related to reward expectancy and delivery than the actual state of the behavior (lick bout initiation). We can also test whether the presence of water influences the firing rate of the cell, by adding a variable containing the state of the reward at the beginning of each lick bout.

More generally, we intend to add all the kinematic variables we have access to so that we can capture all the possible relations between all the variables in single Purkinje cell firing rates. For example, we can use these models to assess how the kinematic variables of the paws, tail, and tongue interact at a single Purkinje cell level to coordinate movement. Do Purkinje cells encode different pieces of information in an additive-like computation? Or are they representing a compound effect of multiple variables that allows decoding different behavioral states? These questions can be tested by evaluating the interactions between variables in the model, informing us how the cerebellum may actually be using high-dimensional information to achieve the optimal motor output.

Bibliography

Albus James S. A theory of cerebellar function // Mathematical Biosciences. feb 1971. 10, 1-2. 25–61.

Apps Richard, Hawkes Richard. Cerebellar cortical organization: a one-map hypothesis // Nature Reviews Neuroscience. sep 2009. 10, 9. 670–681.

Armstrong D M, Edgley S A. Discharges of Purkinje cells in the paravermal part of the cerebellar anterior lobe during locomotion in the cat. // The Journal of Physiology. jul 1984. 352, 1. 403–424.

Armstrong D M, Edgley S A. Discharges of interpositus and Purkinje cells of the cat cerebellum during locomotion under different conditions. // The Journal of Physiology. jun 1988. 400, 1. 425.

Barbour Boris. Synaptic currents evoked in purkinje cells by stimulating individual granule cells // Neuron. oct 1993. 11, 4. 759–769.

Bryant Jerí L., Boughter John D., Gong Suzhen, LeDoux Mark S., Heck Detlef H. Cerebellar cortical output encodes temporal aspects of rhythmic licking movements and is necessary for normal licking frequency // The European journal of neuroscience. jul 2010. 32, 1. 41.

Cao Ying, Maran Selva K., Dhamala Mukesh, Jaeger Dieter, Heck Dr. Detlef H. Behavior-related pauses in simple-spike activity of mouse purkinje cells are linked to spike rate modulation // Journal of Neuroscience. jun 2012. 32, 25. 8678–8685.

Chambers WW, Sprague JM. Functional localization in the cerebellum. I. Organization in longitudinal cortico-nuclear zones and their contribution to the control of posture, both extrapyramidal and pyramidal // The Journal of comparative neurology. 1955. 103, 1. 105–129.

Davis John D., Keehn J. D. Magnitude of reinforcement and consummatory behavior // Science. 1959. 130, 3370. 269–271.

Diener HC, Dichgans J, Guschlbauer B, Bacher M, Rapp H, Klockgether T. The coordination of posture and voluntary movement in patients with cerebellar dysfunction // Movement disorders : official journal of the Movement Disorder Society. 1992. 7, 1. 14–22.

Eccles J. C., Llinás R., Sasaki K. The excitatory synaptic action of climbing fibres on the Purkinje cells of the cerebellum // The Journal of Physiology. jan 1966. 182, 2. 268–296.

Eccles John C., Ito Masao, Szentágothai János. The Cerebellum as a Neuronal Machine. 158, 3807. Berlin, Heidelberg: Springer Berlin Heidelberg, dec 1967. 1439–1440.

Fusi Stefano, Miller Earl K., Rigotti Mattia. Why neurons mix: high dimensionality for higher cognition // Current Opinion in Neurobiology. apr 2016. 37. 66–74.

Heffley William, Hull Court. Classical conditioning drives learned reward prediction signals in climbing fibers across the lateral cerebellum // eLife. sep 2019. 8. 1–21.

Huang Cheng Chiu, Sugino Ken, Shima Yasuyuki, Guo Caiying, Bai Suxia, Mensh Brett D., Nelson Sacha B., Hantman Adam W. Convergence of pontine and proprioceptive streams onto multimodal cerebellar granule cells // eLife. feb 2013. 2013, 2.

Ito M. Neurophysiological aspects of the cerebellar motor control system. // International journal of neurology. 1970. 7, 2. 162–176.

Ito M. Cerebellar long-term depression: Characterization, signal transduction, and functional roles // Physiological Reviews. 2001. 81, 3. 1143–1195.

Ito M. Cerebellar Microcircuitry // Encyclopedia of Neuroscience. jan 2009. 723–728.

James Gareth, Witten Daniela, Hastie Trevor, Tibshirani Robert. An Introduction to Statistical Learning. New York, NY: Springer US, 2021. (Springer Texts in Statistics).

Johnston WJ, Palmer SE, Freedman DJ. Nonlinear mixed selectivity supports reliable neural computation // PLoS computational biology. 2020. 16, 2.

Kiehn Ole. Decoding the organization of spinal circuits that control locomotion. apr 2016. 224–238.

Lee Ka Hung, Mathews Paul J., Reeves Alexander M.B., Choe Katrina Y., Jami Shekib A., Serrano Raul E., Otis Thomas S. Circuit Mechanisms Underlying Motor Memory Formation in the Cerebellum // Neuron. apr 2015. 86, 2. 529–540.

Levin Stephen I., Khaliq Zayd M., Aman Teresa K., Grieco Tina M., Kearney Jennifer A., Raman Indira M., Meisler Miriam H. Impaired Motor Function in Mice With Cell-Specific Knockout of Sodium Channel Scn8a (Na V 1.6) in Cerebellar Purkinje Neurons and Granule Cells // Journal of Neurophysiology. aug 2006. 96, 2. 785–793.

Lisberger SG, Fuchs AF. Role of primate flocculus during rapid behavioral modification of vestibuloocular reflex. I. Purkinje cell activity during visually guided horizontal smooth-pursuit eye movements and passive head rotation // Journal of neurophysiology. 1978. 41, 3. 733–763.

Machado Ana S, Darmohray Dana M, Fayad João, Marques Hugo G, Carey Megan R. A quantitative framework for whole-body coordination reveals specific deficits in freely walking ataxic mice // eLife. oct 2015. 4. 1–22.

Mante Valerio, Sussillo David, Shenoy Krishna V., Newsome William T. Context-dependent computation by recurrent dynamics in prefrontal cortex // Nature 2013 503:7474. nov 2013. 503, 7474. 78–84.

Markanday Akshay, Bellet Joachim, Bellet Marie E., Inoue Junya, Hafed Ziad M., Thier Peter. Using deep neural networks to detect complex spikes of cerebellar Purkinje cells // Journal of Neurophysiology. jun 2020. 123, 6. 2217–2234.

Marr David. A theory of cerebellar cortex // The Journal of Physiology. jun 1969. 202, 2. 437–470.

Mathis Alexander, Mamidanna Pranav, Cury Kevin M., Abe Taiga, Murthy Venkatesh N., Mathis Mackenzie Weygandt, Bethge Matthias. DeepLabCut: markerless pose estimation of user-defined body parts with deep learning // Nature Neuroscience 2018 21:9. aug 2018. 21, 9. 1281–1289.

McFadden Daniel. Quantitative Methods for Analyzing Travel Behaviour of Individuals: Some Recent Developments // Cowles Foundation Discussion Papers. 1977.

Meister Miriam L. R., Hennig Jay A., Huk Alexander C. Signal Multiplexing and Single-Neuron Computations in Lateral Intraparietal Area During Decision-Making // Journal of Neuroscience. feb 2013. 33, 6. 2254–2267.

Morton Susanne, Bastian Amy. Mechanisms of cerebellar gait ataxia // The Cerebellum. 2007. 6, 1. 79–86.

Mullen R. J., Eicher E. M., Sidman R. L. Purkinje cell degeneration, a new neurological mutation in the mouse. // Proceedings of the National Academy of Sciences. jan 1976. 73, 1. 208–212.

Muzzu Tomaso, Mitolo Susanna, Gava Giuseppe P., Schultz Simon R. Encoding of locomotion kinematics in the mouse cerebellum // PLOS ONE. sep 2018. 13, 9. e0203900.

Napper R. M. A., Harvey R. J. Number of parallel fiber synapses on an individual Purkinje cell in the cerebellum of the rat // The Journal of Comparative Neurology. aug 1988. 274, 2. 168–177.

Nath Tanmay, Mathis Alexander, Chen An Chi, Patel Amir, Bethge Matthias, Mathis Mackenzie Weygandt. Using DeepLabCut for 3D markerless pose estimation across species and behaviors // Nature Protocols 2019 14:7. jun 2019. 14, 7. 2152–2176.

Pantò M. R., Zappalà A., Parenti R., Serapide M. F., Cicirata F. Corticonuclear projections of the cerebellum preserve both anteroposterior and mediolateral pairing patterns // European Journal of Neuroscience. feb 2001. 13, 4. 694–708.

Paxinos George, Franklin Keith. Paxinos and Franklin's the Mouse Brain in Stereotaxic Coordinates. 2012. 2nd.

Popa Laurentiu S., Streng Martha L., Ebner Timothy J. Purkinje Cell Representations of Behavior: Diary of a Busy Neuron: // https://doi.org/10.1177/1073858418785628. jul 2018. 25, 3. 241–257.

Purves Dale, Augustine George, Fitzpatrick David, Hall William C., LaMantia Anthony-Samuel, Mooney Richard D., Platt Michael L., White Leonard E. Neuroscience. oct 2017. sixth edit. 427–444.

Rigotti Mattia, Barak Omri, Warden Melissa R., Wang Xiao-Jing, Daw Nathaniel D., Miller Earl K., Fusi Stefano. The importance of mixed selectivity in complex cognitive tasks // Nature. may 2013. 497, 7451. 585–590.

Sarnaik Rashmi, Raman Indira M. Control of voluntary and optogenetically perturbed locomotion by spike rate and timing of neurons of the mouse cerebellar nuclei // eLife. apr 2018. 7. 1–31.

Sauerbrei Britton A., Lubenov Evgueniy V., Siapas Athanassios G. Structured Variability in Purkinje Cell Activity during Locomotion // Neuron. aug 2015. 87, 4. 840–852.

Snider Ray S., Stowell Averill. RECEIVING AREAS OF THE TACTILE, AUDITORY, AND VISUAL SYSTEMS IN THE CEREBELLUM // https://doi.org/10.1152/jn.1944.7.6.331. nov 1944. 7, 6. 331–357.

Sommer Marc A., Wurtz Robert H. Brain Circuits for the Internal Monitoring of Movements // Annual Review of Neuroscience. jul 2008. 31, 1. 317–338.

Streng Martha L., Popa Laurentiu S., Ebner Timothy J. Complex Spike Wars: a New Hope // The Cerebellum. dec 2018. 17, 6. 735–746.

Sugihara I., Wu H., Shinoda Y. Morphology of axon collaterals of single climbing fibers in the deep cerebellar nuclei of the rat // Neuroscience Letters. oct 1996. 217, 1. 33–36.

Thach W T, Goodkin H P, Keating J G. The Cerebellum and the Adaptive Coordination of Movement // Annual Review of Neuroscience. mar 1992. 15, 1. 403–442.

Tsutsumi Shinichiro, Chadney Oscar, Yiu Tin-Long, Bäumler Edgar, Faraggiana Lavinia, Beau Maxime, Häusser Michael. Purkinje Cell Activity Determines the Timing of Sensory-Evoked Motor Initiation // Cell Reports. dec 2020. 33, 12. 108537.

Udo M., Matsukawa K., Kamei H., Minoda K., Oda Y. Simple and complex spike activities of purkinje cells during locomotion in the cerebellar vermal zones of decerebrate cats // Experimental Brain Research. feb 1981. 41-41, 3-4. 292–300.

Wagner Mark J, Kim Tony Hyun, Savall Joan, Schnitzer Mark J, Luo Liqun. Cerebellar granule cells encode the expectation of reward // Nature. 2017. 544, 7648. 96–100.

Walter Joy T, Alviña Karina, Womack Mary D, Chevez Carolyn, Khodakhah Kamran. Decreases in the precision of Purkinje cell pacemaking cause cerebellar dysfunction and ataxia // Nature Neuroscience. mar 2006. 9, 3. 389–397.

Wood Simon N. Fast stable restricted maximum likelihood and marginal likelihood estimation of semiparametric generalized linear models // Journal of the Royal Statistical Society: Series B (Statistical Methodology). jan 2011. 73, 1. 3–36.